NACA RM L57C08

NACA

RESEARCH MEMORANDUM

AN EXPERIMENTAL STUDY AT HIGH SUBSONIC SPEEDS OF SEVERAL TAIL CONFIGURATIONS ON A MODEL HAVING A 45° SWEPTBACK WING

By William C. Sleeman, Jr.

Langley Aeronautical Laboratory
Langley Field, Va.

NATIONAL ADVISORY COMMITTEE
FOR AERONAUTICS

WASHINGTON

April 17, 1957
Declassified July 22, 1959

NACA RM L57C08

NATIONAL ADVISORY COMMITTEE FOR AERONAUTICS

RESEARCH MEMORANDUM

AN EXPERIMENTAL STUDY AT HIGH SUBSONIC SPEEDS OF SEVERAL TAIL CONFIGURATIONS ON A MODEL HAVING A 45° SWEPTBACK WING

By William C. Sleeman, Jr.

SUMMARY

An investigation has been conducted in the Langley high-speed 7- by 10-foot tunnel of the static longitudinal and lateral stability characteristics of a model having a 45° sweptback wing of aspect ratio 4 and having several different tail arrangements. The tail configurations studied had unswept, rectangular surfaces and included a T-tail and conventional fuselage-mounted horizontal and vertical tails. Also tested were Y-tail, H-tail, W-tail, and +-tail configurations. The test Mach number range extended from 0.60 to 0.94, and the angle-of-attack range extended to approximately 25° at the lowest Mach number.

The longitudinal stability characteristics obtained with the various tails were consistent with past experience with swept-wing configurations in that the high tails (T-tail and Y-tail) showed a large pitch-up tendency in the tail contribution at moderate angles of attack. The low tails (H-tail and +-tail) exhibited no destabilizing pitching-moment contribution below an angle of attack of 20°; however, the W-tail, which had essentially all its area below the wing-chord plane, had an appreciable pitch-up tendency in the tail contribution at moderate angles of attack.

An appreciable interference effect on directional stability at low angles of attack and high Mach numbers was noted for the T-tail, the Y-tail, and the conventional fuselage-mounted tail. This interference was most pronounced with the tapered afterbody and was evidenced by a fairly large variation in directional stability with angle of attack at low angles as the Mach number was increased. Modifications of the fuselage afterbody from a moderately tapered shape to a cylindrical shape effected a significant reduction in this adverse interference. For all the tail configurations studied, significant losses in tail contribution to directional stability were experienced as the angle of attack increased; however, there were marked differences in the manner in which these losses occurred for the various tail configurations.

INTRODUCTION

The present investigation was made to supplement the study (ref. 1) of tail configurations on a straight-wing model by including additional types of tail configurations on a sweptback-wing model. The primary interest in conducting the present study was to obtain a swept-wing airplane configuration which would retain positive directional stability throughout the range of angle of attack by use of either conventional or unusual tail arrangements. The configurations investigated included a T-tail, a Y-tail, an H-tail, a W-tail, a +-tail, and a fuselage-mounted conventional tail formed by removing the bottom fin of the +-tail. The effects of fuselage afterbody shape on the aerodynamic characteristics of the model were investigated with some of the tail arrangements by use of a cylindrical fuselage afterbody in addition to the basic tapered afterbody.

Static longitudinal and lateral stability characteristics were determined for the model with the various tail configurations for Mach numbers from 0.60 to 0.94 and for a range of angle of attack up to approximately 25° at the lowest Mach numbers. The wing used in the present tests had an aspect ratio of 4, a taper ratio of 0.30, and a quarter-chord sweep of 45°. All the tails investigated were of rectangular plan form and were unswept.

SYMBOLS

The lateral stability results of this investigation are referred to the body-axis system which is shown in figure 1 together with an indication of positive directions of forces, moments, and displacements of the model. The lift and drag characteristics presented at 0° sideslip are, respectively, normal and parallel to the relative wind as shown in the side view of the model given in figure 1. Moment coefficients are given about the reference center shown in figure 2 (located on the fuselage center line at a longitudinal position corresponding to the 25-percent wing mean aerodynamic chord.)

C_L lift coefficient, $\frac{\text{Lift}}{qS}$

C_D drag coefficient, $\frac{\text{Drag}}{qS}$

C_m pitching-moment coefficient, $\frac{\text{Pitching moment}}{qS\bar{c}}$

C_l rolling-moment coefficient, $\frac{\text{Rolling moment}}{qSb}$

C_n yawing-moment coefficient, $\frac{\text{Yawing moment}}{qSb}$

C_Y lateral-force coefficient, $\frac{\text{Lateral force}}{qS}$

q dynamic pressure, $\frac{\rho V^2}{2}$, lb/sq ft

V velocity, ft/sec

ρ air density, slugs/cu ft

M Mach number

S wing area, 0.25 sq ft

b wing span, 1.0 ft

$\bar{c}$ wing mean aerodynamic chord, 0.274 ft

α angle of attack of fuselage center line, deg

β angle of sideslip, deg

i_t stabilizer incidence measured in plane of symmetry (positive for trailing edge down), deg

Subscripts:

β denotes partial derivative of a coefficient with respect to sideslip, for example $C_{l_\beta} = \frac{\partial C_l}{\partial \beta}$

t denotes increment due to addition of tail surfaces

MODEL AND APPARATUS

Model Description

The wing-fuselage arrangement used in this investigation for all the tail configurations is shown in figure 2, and details of the tapered

and cylindrical afterbodies are given in figure 3. The steel wing of the model had an aspect ratio of 4, a taper ratio of 0.30, quarter-chord sweep of 45°, and NACA 65A006 airfoil sections parallel to the free-stream direction.

Tail 1 is shown on the model in figure 2, and all the tails had the same longitudinal location as tail 1. Sketches showing a rear view of the various tails on the fuselage are given in figure 4. In figure 4 the outer fuselage diameter shown represents the base of the cylindrical afterbody and the inner circle denotes the base diameter of the tapered afterbody. All the tails had a chord of 1.8 inches and NACA 65A006 airfoil sections. The tails were constructed of steel and were soldered to interchangeable fuselage blocks.

Apparatus

The present tests were made with the model mounted on a remotely controlled variable-angle yaw sting. Use of this sting enabled continous records of forces and moments to be obtained while the model slowly traversed the angle-of-sideslip range. The automatic sting controls were devised so that the yawing cycle was interrupted at sideslip angles of approximately 0° and ±5°; test data points were obtained while these angles of sideslip were held constant. Further description of the variable-angle yaw sting may be found in reference 2.

TESTS AND RESULTS

Test Conditions

Tests were conducted in the Langley high-speed 7- by 10-foot tunnel over a Mach number range from 0.60 to 0.94 and an angle-of-attack range from -2° to approximately 25° at the lowest test Mach numbers. All the configurations were tested at sideslip angles of approximately 0° and ±5° at constant values of angle of attack. Data at the highest test Mach number were not obtained at angles of attack below approximately 2°. This angle restriction was due to the excessively high drag of the model support and hydraulic lines mounted to the rear part of the sting which was inclined -12° at a model angle of attack of 0°.

The average test Reynolds number based on the wing mean aerodynamic chord varied from approximately 0.92×10^6 for the lowest to 1.15×10^6 for the highest test Mach numbers.

No jet-boundary or blockage corrections have been applied to the data inasmuch as the model size relative to the size of the tunnel test section was very small. Corrections to the angles of attack and sideslip angles due to deflection of the strain-gage balance and support system under load have been applied. No base-pressure corrections have been applied to the drag coefficients presented herein.

Presentation of Results

Aerodynamic characteristics in pitch for the wing-fuselage configuration and the tail-on arrangements are presented in figures 5 to 11. Lateral stability derivatives obtained when the assumption of a linear variation of lateral components with sideslip between $\beta = \pm 5^{\circ}$ is used are presented in figures 12 to 18. As mentioned previously, continuous records of forces and moments were obtained throughout the test sideslip range, and for the most part the lateral components showed a linear variation between $\pm 5^{\circ}$ sideslip. In some cases at moderately high angles of attack, nonlinearities were encountered in the lateral components, particularly rolling moments, and for these cases the derivatives obtained at $\pm 5^{\circ}$ sideslip may have decreased significance. A fairly complete discussion of these nonlinearities and where they occurred for an unswept-wing model are given in reference 2. Tail contributions to pitching moments and to directional stability are presented in figures 19 and 20, and effects of angle-of-attack changes on the tail contributions are summarized in figure 21. A comparison is made in figure 22 of the directional stability and tail contribution to directional stability for some of the tail configurations of the present swept-wing model and the unswept model of reference 1.

DISCUSSION

Wing-Fuselage Characteristics

Aerodynamic characteristics in pitch for the wing-fuselage configuration with the two afterbody shapes are presented in figure 5 and show the typical unstable break in pitching moments at moderate lift coefficients characteristic of thin, highly sweptback wings. Some of the tail arrangements tested were therefore selected on the basis of past experience to provide a contribution to longitudinal stability which would overcome the pitch-up tendency of the wing-fuselage configuration and give a more linear pitching-moment variation for the complete model.

Lateral stability derivatives for the wing-fuselage configuration are given in figure 12 and show variations with angle of attack typical

of those for highly swept, thin-wing—fuselage combinations. The increase in directional instability at moderately high angles of attack shown in figure 12 is opposite to that encountered for the unswept wing-fuselage combination of reference 1 which became directionally stable at high angles of attack. Reasons for these differences in stability are discussed in reference 3. The basic difference in tail-off directional stability at high angles of attack for the swept and unswept configurations places the complete model with the swept wing at a comparative disadvantage because the tail contribution required to maintain a given positive value of directional stability will have to increase with angle of attack for the swept configuration. On the other hand, the decrease in tail contribution at high angles of attack which normally occurs for conventional vertical tails is at least partially offset on the unswept configuration of reference 1 by the stable shift in the wing-fuselage characteristics. Comparisons of directional stability characteristics in this report of the swept and unswept configurations will therefore be made on the basis of both tail contribution and overall complete-model stability.

Effects of Afterbody Shape

Longitudinal characteristics.- Aerodynamic characteristics in pitch for the wing-fuselage configuration presented in figure 5 show no significant effects of afterbody shape on the lift characteristics. The drag data of figure 5, however, show an increment of about 0.01 higher drag coefficients obtained with the cylindrical afterbody than with the tapered afterbody over the low and moderate lift-coefficient range. This increment in drag due to afterbody shape also appears in the tail-on data and is believed to be due to differences in base drag. Base-pressure corrections were not applied to the drag data inasmuch as measurements of base pressures were not obtained in this investigation.

Effects of afterbody shape on pitching moments were not pronounced; however, the pitching moments obtained with the cylindrical afterbody were generally more negative than those obtained with the tapered afterbody (fig. 5 and figs. 7 to 11).

Lateral stability.- The effects of fuselage afterbody shape on the lateral stability derivatives are shown in figures 12 to 16. These results show essentially no effect of afterbody shape on C_{l_β}; however, an appreciable effect is noted for derivatives C_{n_β} and C_{Y_β}. The wing-fuselage characteristics presented in figure 12 show somewhat smaller negative values of C_{n_β} at low angles of attack for the model with the cylindrical afterbody than the tapered-afterbody configuration,

and this smaller negative value is accompanied by correspondingly greater values of the derivative C_{Y_β} for the model with the cylindrical afterbody. These results indicate that the forces producing the body instability were altered by making the afterbody cylindrical and thereby reducing the afterbody contribution to the overall body instability. The loading caused by the sloping afterbody is opposite in sign to that produced by the body nose, and a reduction of this afterbody load by eliminating the slope would be expected to result in a net increase in force in the direction of the force on the body nose. This condition may explain the fact that C_{Y_β} became more negative (loss of positive C_{Y_β} contribution of the afterbody) as C_{n_β} became less negative. In addition to this effect a stabilizing increment might be realized because of an increase in crossflow separation on the cylindrical afterbody compared with the tapered afterbody; however, this effect of afterbody shape would be expected to be very small at low angles of attack and sideslip.

The most significant effect encountered, relative to changes in afterbody shape, was the relieving effect of the cylindrical afterbody on the Mach number interference influencing certain of the tail configurations tested; for example, the directional stability characteristics with the Y-tail (tail 6) at -6° incidence and the tapered afterbody (fig. 16) show a decrease in C_{n_β} at an angle of attack of 0° as the Mach number increases. This directional-stability loss at low angles of attack and the attendant large variation of C_{n_β} with angle of attack shows generally the same trends as those encountered with this same Y-tail used in the tests of reference 1. Test results obtained with the Y-tail, the cylindrical afterbody, and a negative stabilizer setting showed a considerable increase in directional stability when compared with results for the tapered afterbody up to at least an angle of attack of 15°, particularly at the higher Mach numbers. In addition to the effect of afterbody shape for the negative stabilizer setting (fig. 16), a large effect of stabilizer incidence is indicated with the cylindrical afterbody configuration and similar effects would also be expected for the tapered afterbody, based on the present results and those of reference 1. As noted in reference 1, the interference effects appear to be a function of horizontal-tail angle of attack, and negative increments in either stabilizer setting or angle of attack produced losses in directional stability at low angles of attack. These interference effects are believed to be a further manifestation of the interference of the V-portion of the tail, the vertical stub, and the fuselage afterbody upon each other which cause shock formation and flow breakdown. Although not verified experimentally, it appears from the present results and those of reference 1 that the cylindrical afterbody would also have a relieving effect on the losses in C_{n_β} due to

negative increments in stabilizer setting. Furthermore, it also appears that effects of afterbody shape and stabilizer setting encountered on the Y-tail of the present tests are indicative of those to be expected for the T-tail. For additional information on these losses in directional stability, reference is made to the discussion of interference effects in reference 1.

In addition to the Mach number interference effects encountered on the Y-tail, these effects also appeared to a lesser extent with tails 2 and 3. Directional stability characteristics presented in figures 13 and 14 show an increasing difference between results for the tapered afterbody and the cylindrical afterbody with increasing Mach number. Test results throughout the Mach number range for the cylindrical afterbody (figs. 13 and 14) show very little increase in C_{n_β} with angle of attack whereas results for the tapered afterbody show an overall tendency to increase with angle of attack up to approximately 10°. This difference in characteristics for the two afterbodies is believed to result from interference effects present with the tapered afterbody and is probably due to mutual interference of the horizontal tail, the vertical tail, and the afterbody inasmuch as results without the horizontal tail (tail 9, fig. 18) at $M = 0.94$ show only a slight increase in stability with angle of attack up to 10°.

Directional stability characteristics of the model with the H-tail (tail 5) showed no significant effects of the afterbody shape (fig. 15) throughout the test Mach number range. The absence of afterbody-shape effects and horizontal-tail interference, as indicated for other configurations, may be explained for the H-tail by the fact that the vertical tail was located away from the fuselage and was therefore less influenced by local fuselage and horizontal-tail interference.

Effect of Tail Configuration on Stability

Longitudinal stability.- The pitching-moment contribution of the tail surfaces tested is summarized in figure 19. In general, as would be expected for the present swept-wing configuration, tail arrangements appreciably above the wing-chord plane (tail 1 and tail 6) showed an appreciable pitch-up tendency at moderately high angles of attack, whereas results for the tails located in a low position generally showed a stabilizing break in tail contribution. For a Mach number of 0.60, the tail contribution to pitching moments was stabilizing for all the tails located on the wing-chord plane for angles of attack up to 22° (fig. 19). The appreciable end-plate effect of the vertical tails on the H-tail can be seen from the increase in pitching-moment slope of tail 5 as compared with tail 2 or tail 3, for example.

The pitching-moment contribution of the W-tail shows a marked pitch-up tendency at high angles of attack for $M = 0.60$ and at relatively low angles of attack for $M = 0.90$ (fig. 19). This destabilizing break in tail contribution would not be expected for a conventional horizontal tail, on the basis of the vertical location of the tail, inasmuch as most of the tail was well below the wing-chord plane. A possible explanation of this adverse tail contribution for the W-tail may be found by a consideration of sidewash effects on the tail panels having dihedral. The favorable effect of sidewash from the wing-tip vortices for a V-tail (mounted well above the wing-chord plane) configuration has been discussed at some length in reference 4, and utilization of the concepts of reference 4 gives a plausible explanation of the pitching-moment behavior of the model with the W-tail. From a consideration of only the wing-tip vortices, the sidewash above the wing wake would be toward the plane of symmetry, and the sidewash below the wake would be directed toward the wing tip. Under these conditions the outer panels of the W-tail placed below the wing would experience a down load produced by sidewash and positive tail dihedral as well as by the downwash flow component. In a similar manner the inboard panels having negative dihedral would experience an up load induced by sidewash and a down load caused by downwash. For the present model, effects on the outer panels would be expected to predominate, inasmuch as these panels had almost twice the span of the inner panels and were closer to the wing-tip vortices.

Lateral stability.- The effects of horizontal-tail height on the tail contribution to directional stability are shown in figure 20. A comparison of results at $M = 0.60$ for tail 1 and tail 2 shows that the vertical-tail contribution was increased at least 25 percent over the angle-of-attack range by moving the horizontal-tail position from the fuselage center line to the tip of the vertical tail. The end-plate effect of the high horizontal tail decreased substantially at the higher Mach numbers near $\alpha = 0^\circ$, as was noted for this tail arrangement in the results of reference 1 with the unswept wing model.

The contribution of tail 5 to directional stability indicated some interesting effects of tail configuration with regard to the contribution at an angle of attack of 0° and to changes throughout the range of angle of attack. The arrangement of tail 5 was selected to locate the vertical stabilizing surfaces away from the influence of the fuselage as much as possible. This selection was made in an attempt to avoid regions of high sidewash emanating from the fuselage vortices and to reduce or eliminate the large losses in directional stability normally encountered at high angles of attack. A comparison of the configurations of tail 5 and tail 4 (fig. 4) shows that these tails had about the same exposed vertical-tail area; however, the contribution to directional stability at $\alpha = 0^\circ$ for the H-tail (tail 5) was less than one-half of that for the +-tail (tail 4). This reduction in tail contribution

was caused by the effects of a smaller aspect ratio on the vertical-tail lift slope for the H-tail compared with that of the +-tail. Both tail 3 and tail 9, which had about one-half the exposed vertical-tail area of tail 5, had approximately the same tail contribution to directional stability at low angles of attack as tail 5. This fact indicates that the fuselage provided a significant end-plate effect on the vertical-tail contribution, and a comparison of results for tail 3 and tail 9 indicates that the horizontal tail located on the fuselage center line provided essentially no additional end-plate effect on the vertical tail over that provided by the fuselage.

The low vertical position of the W-tail was expected to afford advantages from the standpoint of directional stability at high angles of attack. The contribution of tail 8 to directional stability was relatively invariant with angle of attack; however, the overall level of its contribution was rather low (fig. 20). Addition of the top fin (same as that of tail 9) to tail 8 to form tail 7 provided an appreciable increment in tail contribution at an angle of attack of 0°, but the decrease in tail contribution at high angles of attack for the vertical tail (tail 9) is reflected in the characteristics of tail 7.

Thus far, the effects of tail configuration on the level of tail contribution to directional stability at low angles of attack have been emphasized. Further consideration is now given to the influence of tail arrangements on the variation of directional stability through the range of angle of attack. The tail contributions of figure 20 have been normalized at an angle of attack of 0° to indicate more clearly the comparative effects of tail configuration, and these results are given in figure 21. Most of the configurations tested experienced large losses in tail contribution at moderate or high angles of attack as shown in figure 21. The Y-tail and the W-tail showed the smallest overall losses over the angle-of-attack range up to about 24°; however, indications are that further increases in angle of attack would result in large losses in tail contribution.

The characteristics shown in figure 21 at $M = 0.60$ for the H-tail (tail 5) show trends which are different than those for the other tail arrangements. These results show a comparatively early rapid decrease in tail contribution ($\alpha = 6^\circ$) and an attendant large loss followed by a rapid increase in contribution up to the maximum angle of attack. This difference in behavior for the H-tail may be attributed to the effects of sidewash over the vertical tails emanating from the tip vortex of the leading-wing panel in sideslip. At low angles of attack, where the vortex strength is relatively low, the sidewash effects on the upper and lower halves of the vertical tail would tend to cancel each other. At somewhat higher angles of attack, however, the tail would move down in relation to the vortex center, and the resulting sidewash from the lower side of the vortex would be destabilizing.

Further increases in angle of attack would be expected to cause the tail to move below the strongest wing-tip vortex-induced sidewash and into a more favorable flow region to give an increasing tail contribution to directional stability.

Comparison of Swept- and Unswept-Wing Configurations

Some of the test results obtained in the present study were obtained with the same tail arrangements used in the investigation of the unswept-wing model of reference 1. A brief comparison of both longitudinal and directional characteristics is made herein to illustrate the differences obtained in results with these two wings.

Longitudinal stability.- Inasmuch as the comparison of pitching moments for the swept and unswept configurations is fairly straightforward, results from reference 1 are not repeated herein. The comparison of longitudinal characteristics shows the overall effects of tail height to be expected on the basis of past experience. The high-tail configurations (T-tail and Y-tail) showed an earlier onset of instability and more extensive range of destabilizing tail contribution when tested with the swept wing than with the unswept wing. The low-tail arrangement (tail 4), however, provided a more satisfactory tail contribution over the angle-of-attack range with the swept wing than with the unswept wing, particularly at the highest test Mach number.

Directional stability.- The directional stability characteristics of the complete model and the tail contribution of reference 1 have been converted to the body-axis system and the coefficients converted to the reference area and span of the present tests. A comparison of both the tail contribution and overall directional stability of the complete models is given in figure 22 for $M = 0.60$. Figure 22 shows that the tail contribution for the Y-tail (tail 6) was greater with the swept wing at high angles of attack than with the unswept wing. The greater instability of the swept-wing—fuselage configuration (tail-off) at the highest angles, however, tended to make the overall stability of the complete swept configuration less than that of the unswept model. The tail contribution for the +-tail was somewhat lower behind the swept wing than behind the unswept wing, and this difference combined with the aforementioned large instability in the tail-off characteristics at high angles for the swept model and caused a large destabilizing increment in overall directional stability when changing from the unswept to the swept-wing model.

SUMMARY OF RESULTS

An investigation at high subsonic speeds of several different tail arrangements on a model having a 45° sweptback wing indicated the following results:

1. The longitudinal stability characteristics encountered were consistent with past experience on swept-wing configurations in that the high tails (T-tail and Y-tail) showed a large pitch-up tendency in the tail contribution at moderate angles of attack. The low tails (H-tail and +-tail) exhibited no destabilizing contribution below an angle of attack of 20°.

2. The W-tail, which had essentially all its area below the wing-chord plane, exhibited an appreciable pitch-up tendency in the tail contribution at moderate angles of attack.

3. An appreciable interference effect on directional stability at angles of attack near 0° was noted for the T-tail, the Y-tail, and the conventional fuselage-mounted tail at the highest test Mach numbers. This interference was most pronounced with the tapered afterbody and was evidenced primarily by a fairly large variation in directional stability with angle of attack at low angles. In some cases this interference was also evidenced by a loss in stability at an angle of attack of 0° at the higher Mach numbers.

4. Modification of the fuselage afterbody shape from moderately tapered to cylindrical effected a significant reduction in the high Mach number interference on directional stability encountered at low angles of attack.

5. All the tail configurations experienced significant losses in tail contribution to directional stability in changing from low to high angles of attack at a Mach number of 0.60 where the maximum range of angle of attack was covered. There were, however, marked differences in the manner in which these losses occurred for the various tail configurations. The Y-tail and W-tail configurations, for example, showed the smallest overall losses in changing from low to high angles of attack up to 24°; however, indications are that a further increase in angle of attack would result in large losses in tail contribution. The H-tail configuration, on the other hand, showed a large early decrease

in tail contribution followed by stabilizing increases at higher angles of attack.

Langley Aeronautical Laboratory,
National Advisory Committee for Aeronautics,
Langley Field, Va., February 15, 1957.

REFERENCES

1. Sleeman, William C., Jr.: An Experimental Study at High Subsonic Speeds of Several Tail Configurations on a Model With an Unswept Wing. NACA RM L56A06a, 1956.

2. Hayes, William C., Jr., and Polhamus, Edward C.: Wind-Tunnel Investigation of the Effects of Wing Thickness on the Static Longitudinal and Lateral Stability of Unswept Wings of Aspect Ratio 3 at High Subsonic Speeds. NACA RM L56E30a, 1956.

3. Polhamus, Edward C., and Spreemann, Kenneth P.: Subsonic Wind-Tunnel Investigation of the Effect of Fuselage Afterbody on Directional Stability of Wing-Fuselage Combinations of High Angles of Attack. NACA TN 3896, 1956.

4. Polhamus, Edward C., and Moss, Robert J.: Wind-Tunnel Investigation of the Stability and Control Characteristics of a Complete Model Equipped With a Vee Tail. NACA TN 1478, 1947.

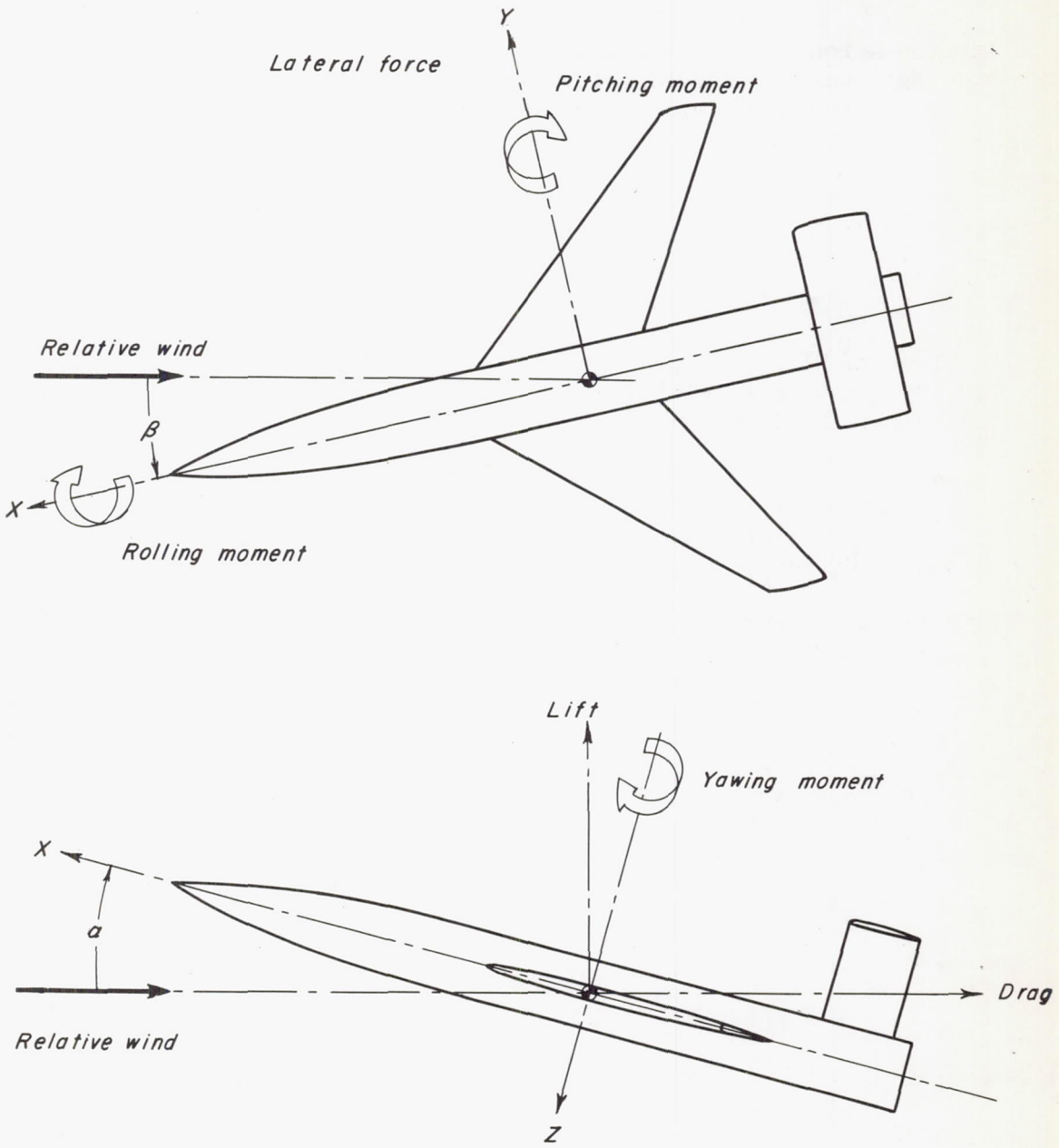

Figure 1.- Body reference axes showing positive directions of forces, moments, and angular deflections.

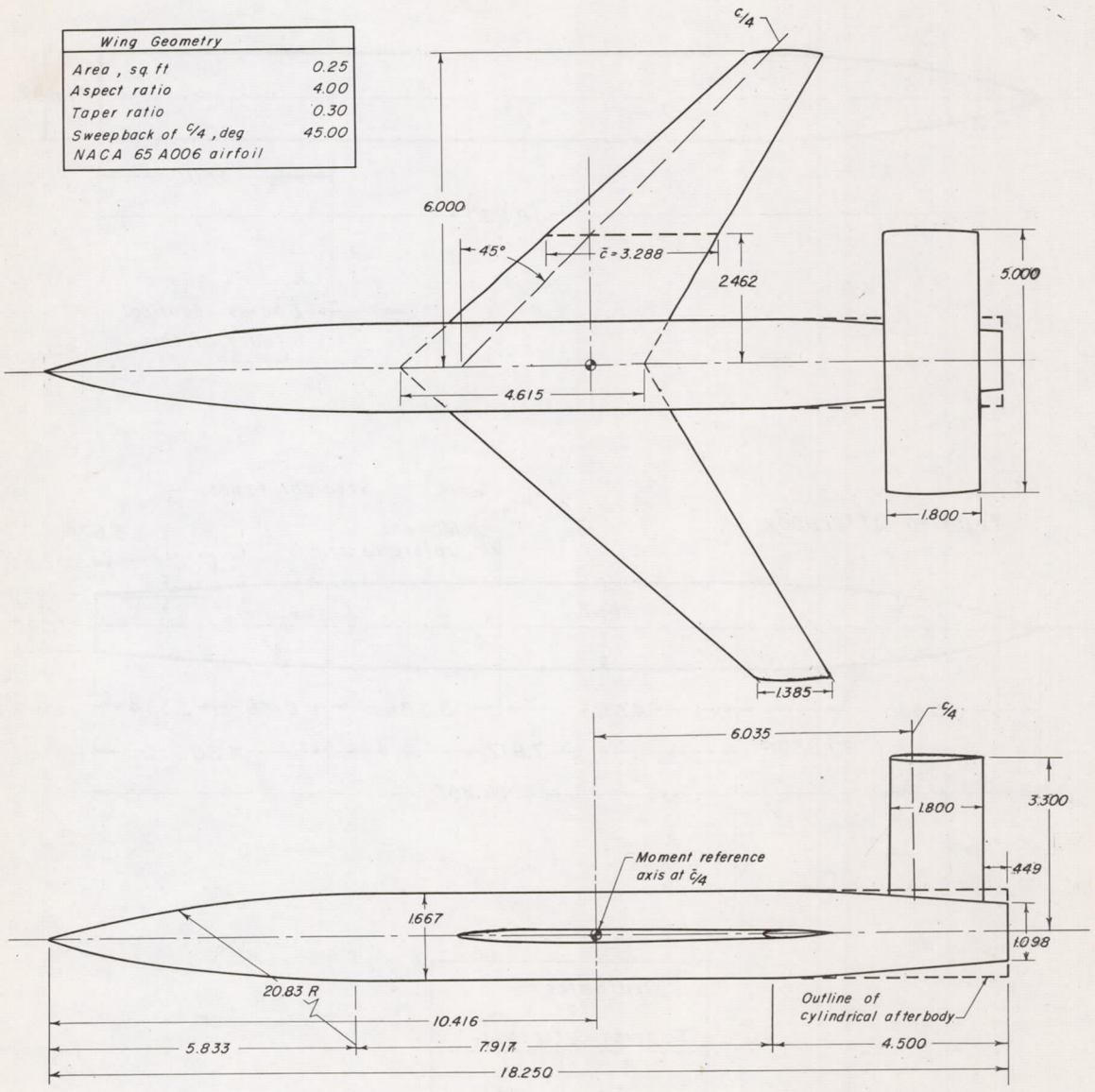

Figure 2.- General arrangement of the model showing tail 1 in place. Linear dimensions are in inches.

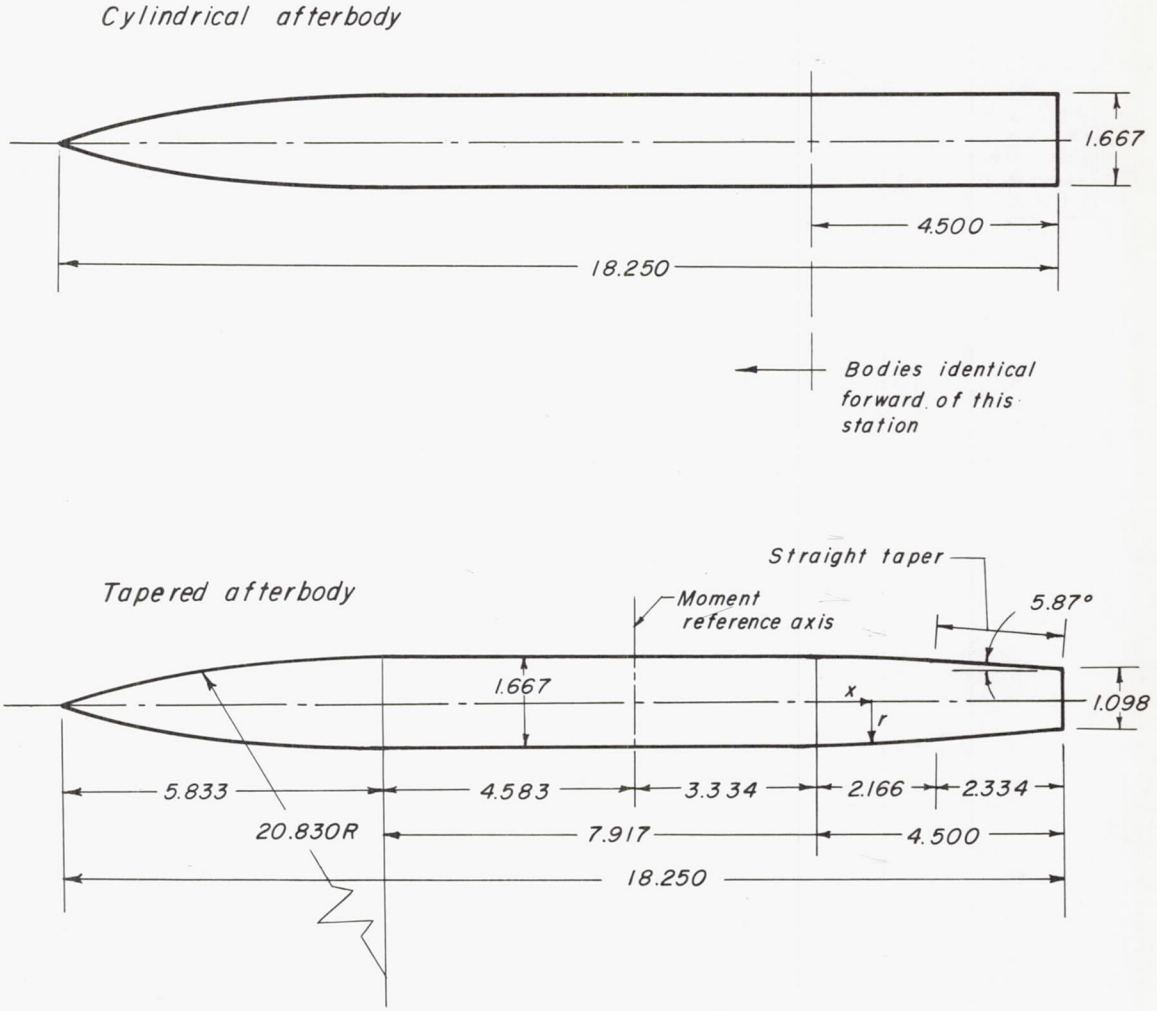

Ordinates for Tapered afterbody	
x	r
0	.833
.584	.812
1.166	.779
2.166	.712
Linear taper to base	
4.500	.549

Figure 3.- Details of the two fuselage afterbodies tested. Linear dimensions are in inches.

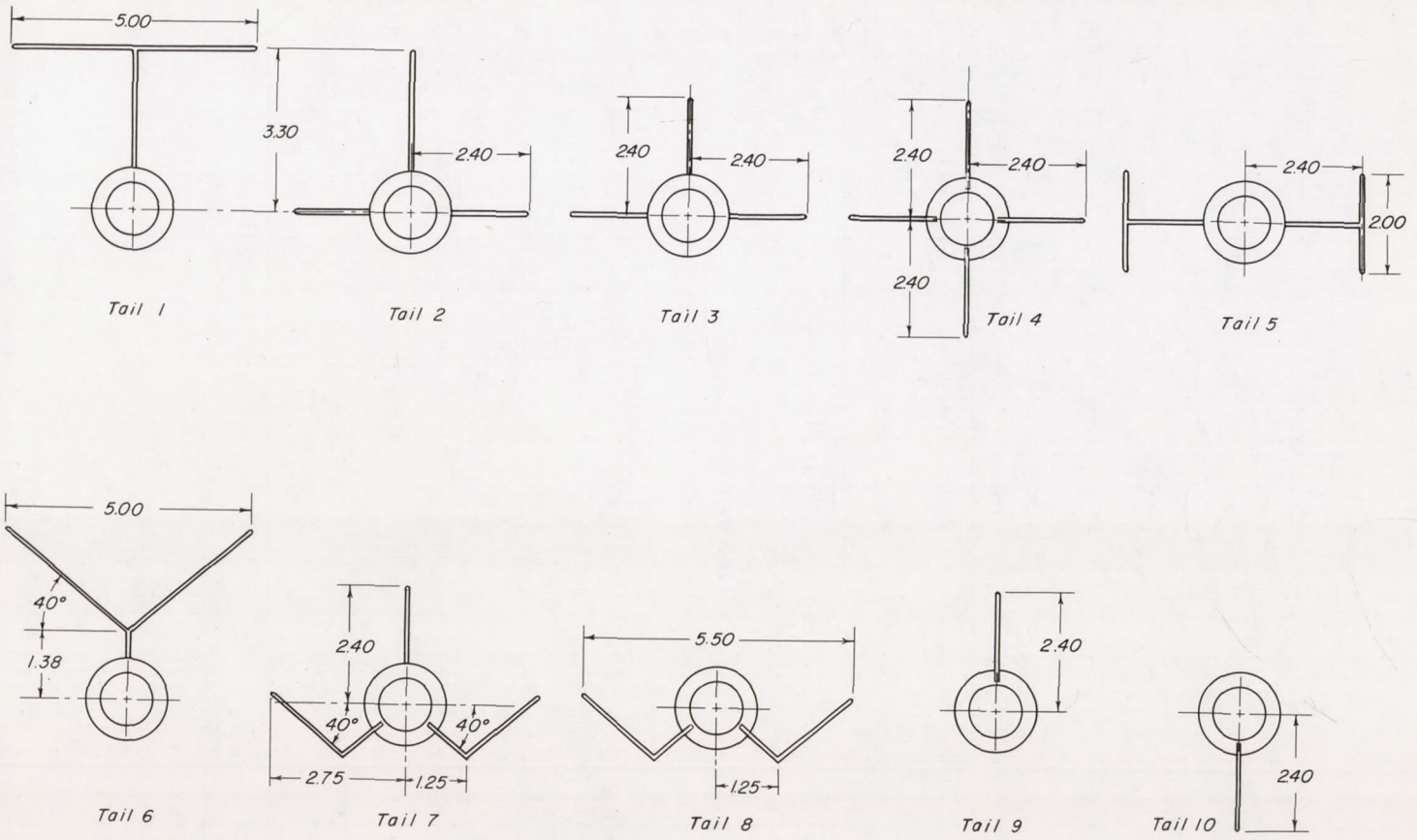

Figure 4.- Rear view of the various tail configurations tested. Linear dimensions are in inches.

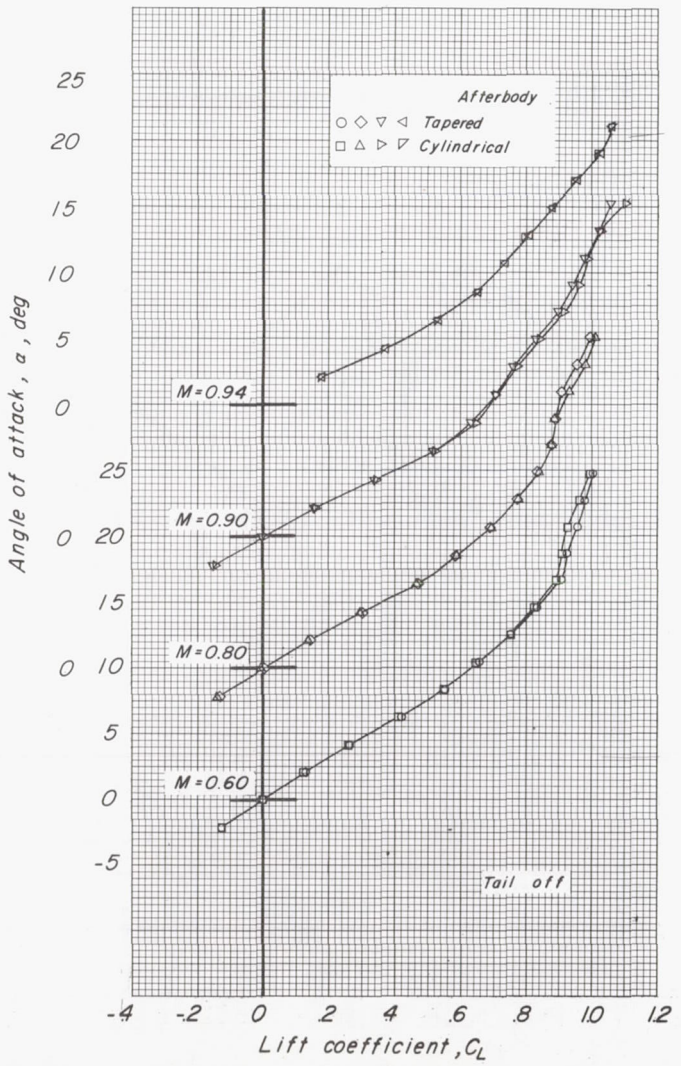

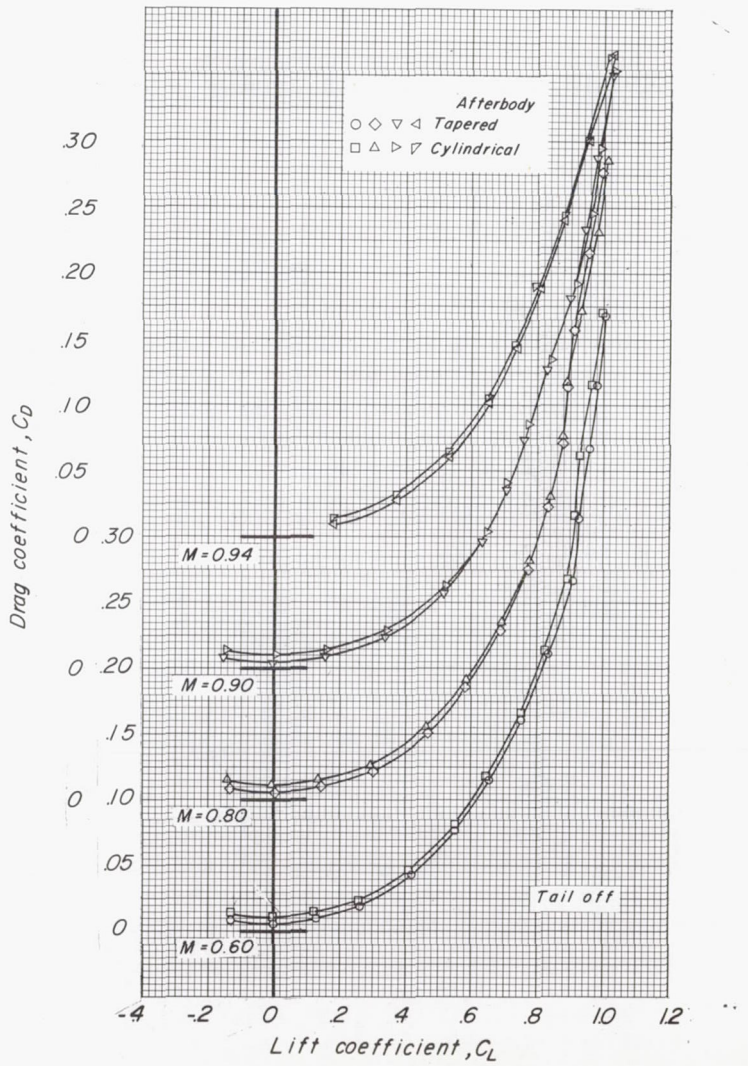

Figure 5.- Aerodynamic characteristics in pitch for the wing-fuselage configurations.

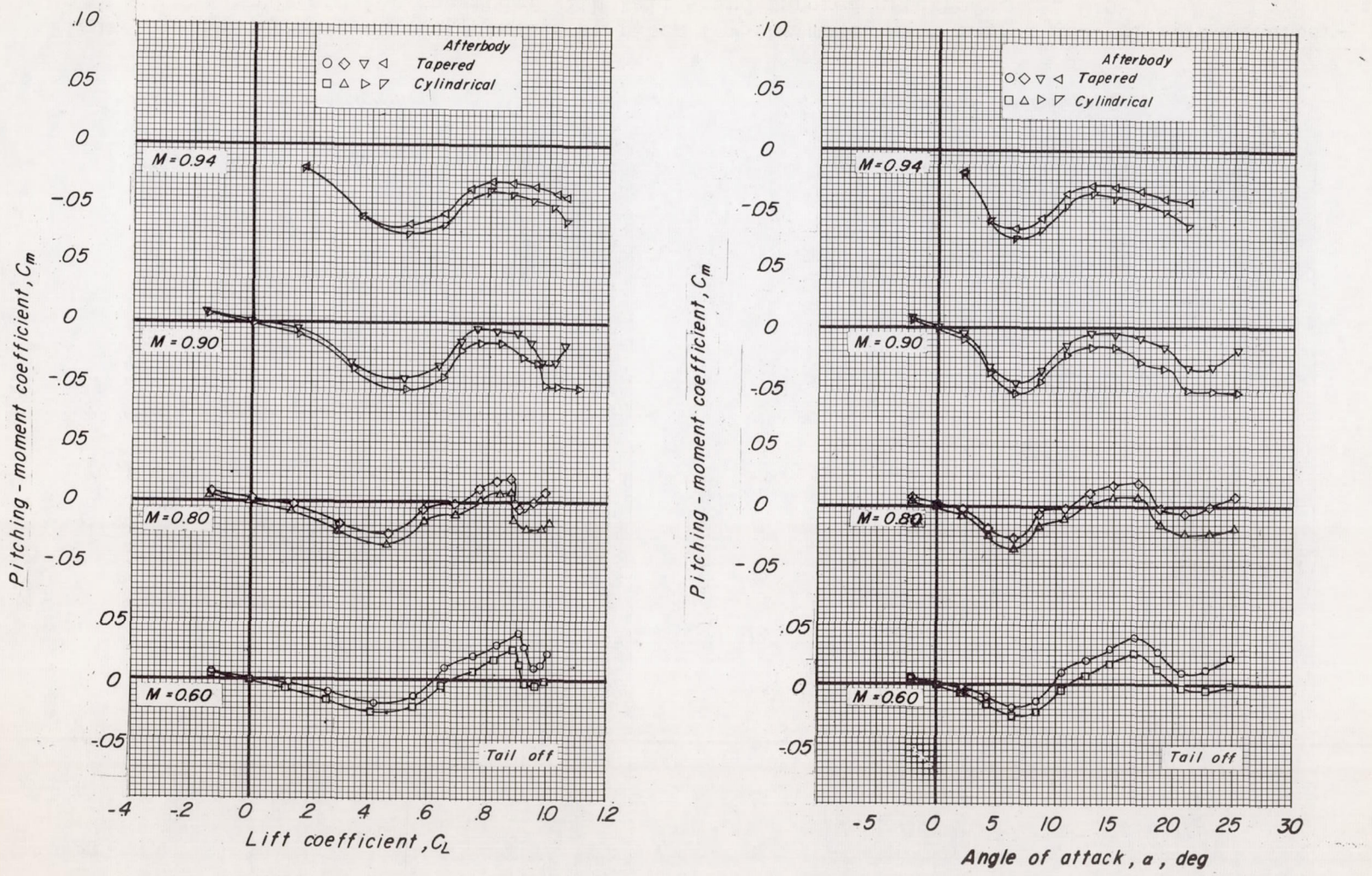

Figure 5.- Concluded.

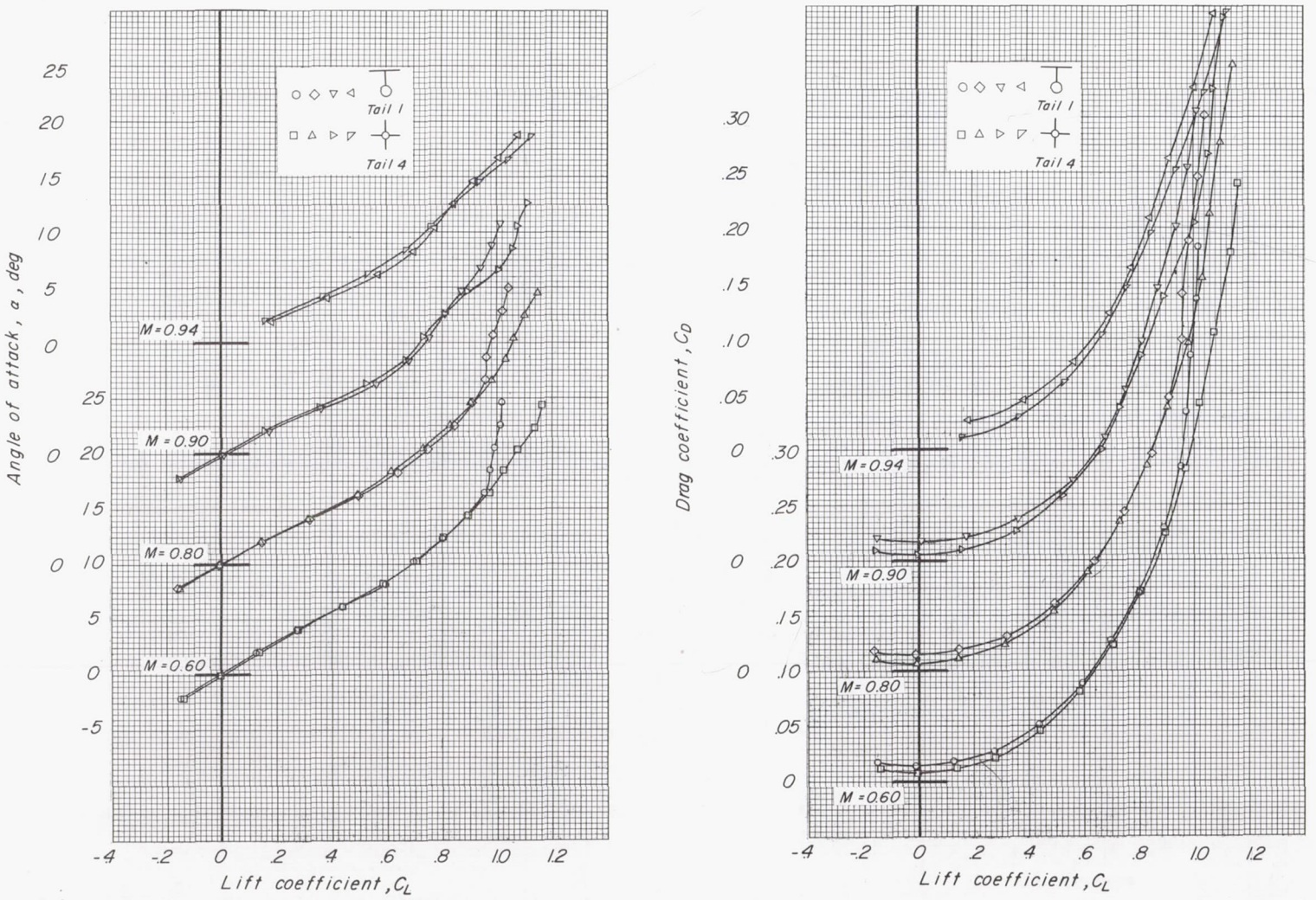

Figure 6.- Aerodynamic characteristics in pitch for the model with tail 1 and cylindrical afterbody and for the model with tail 4 and tapered afterbody. $i_t = 0^\circ$.

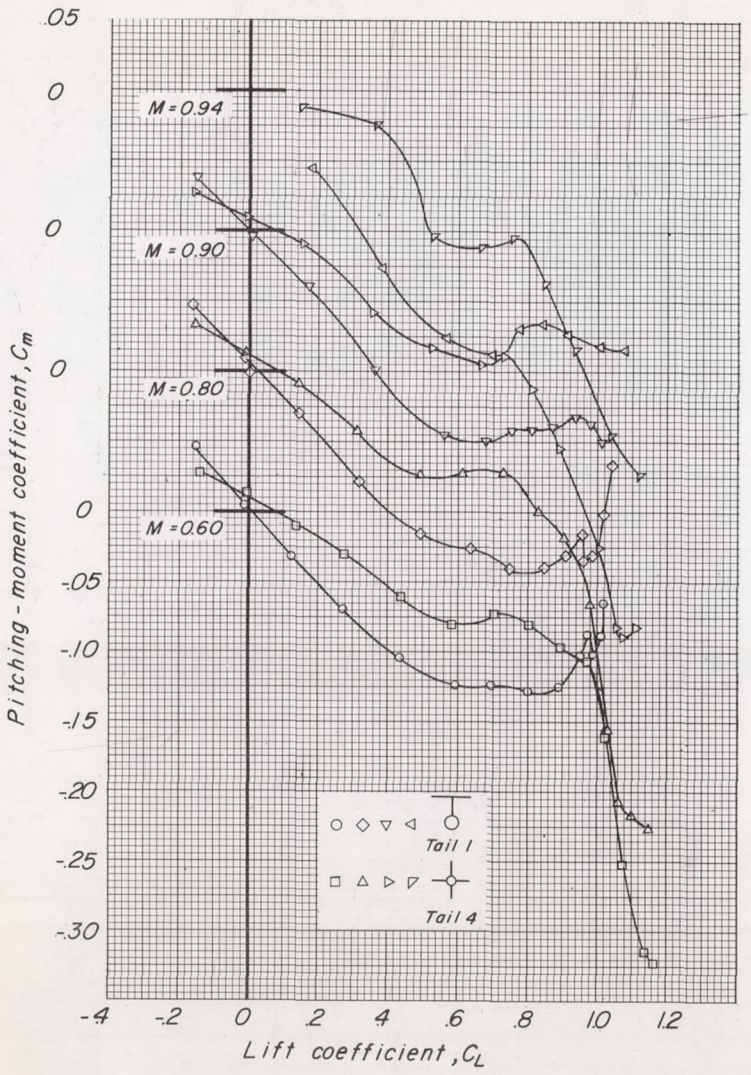

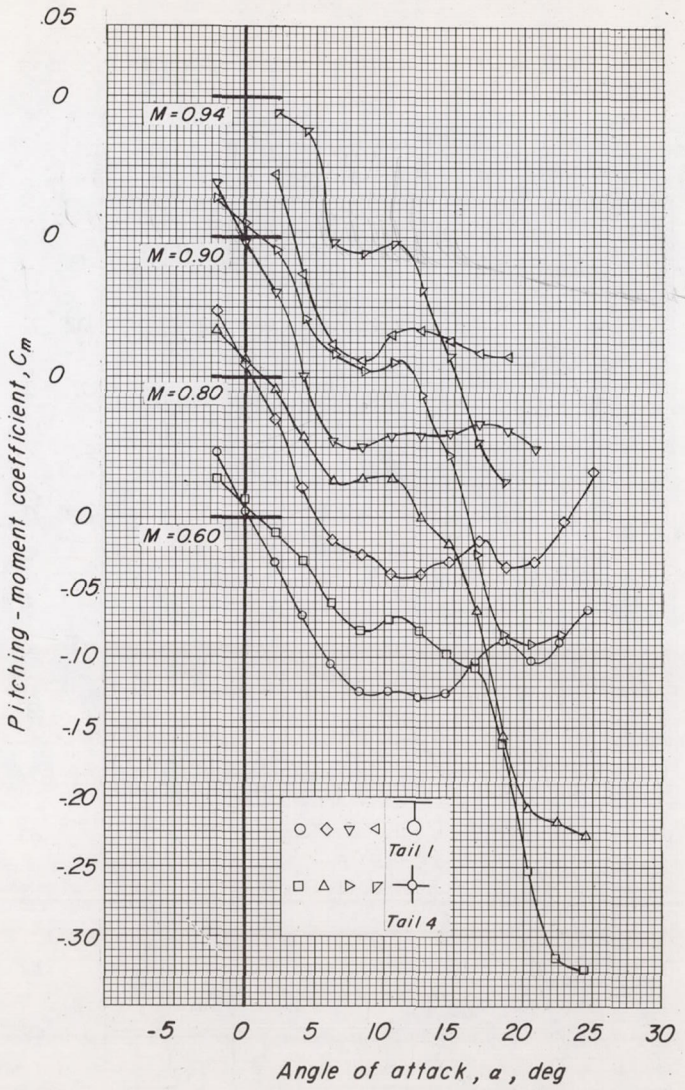

Figure 6.- Concluded.

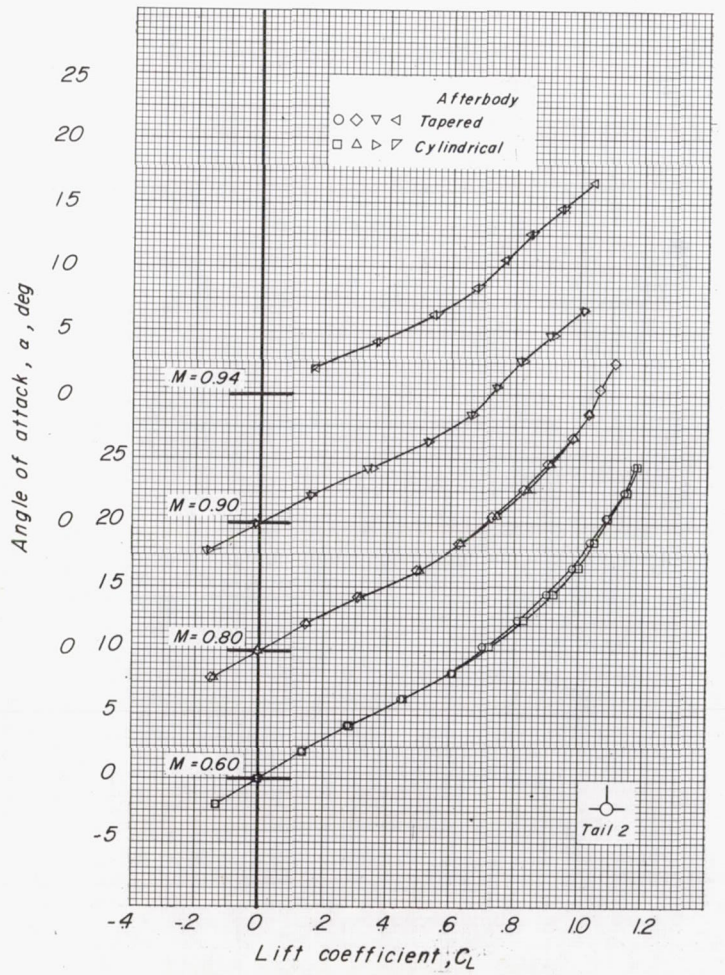

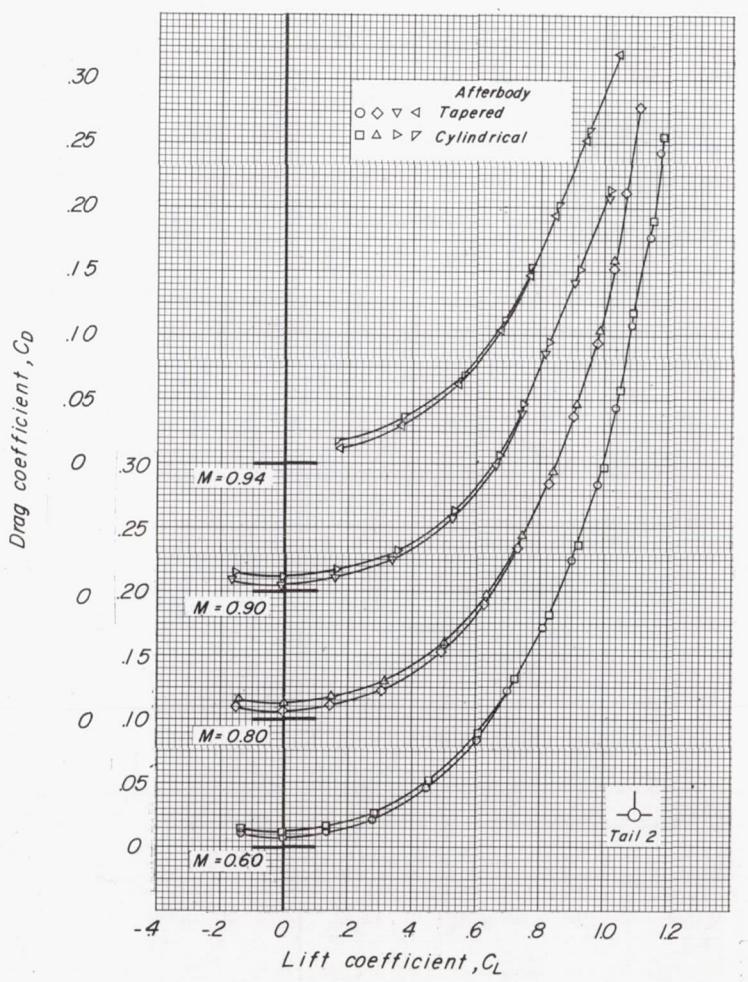

Figure 7.- Aerodynamic characteristics in pitch for the model with tail 2. $i_t = 0^\circ$.

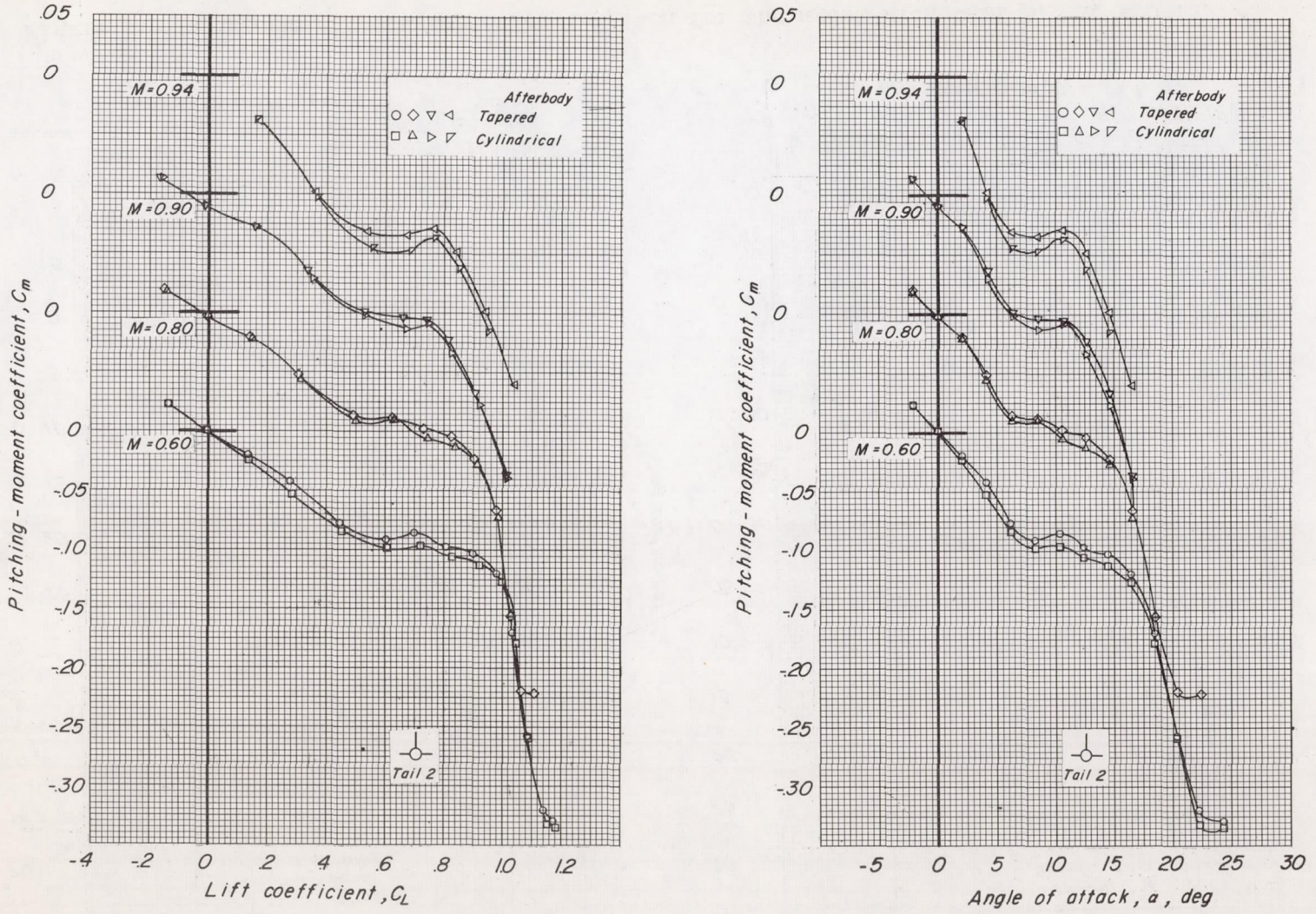

Figure 7.- Concluded.

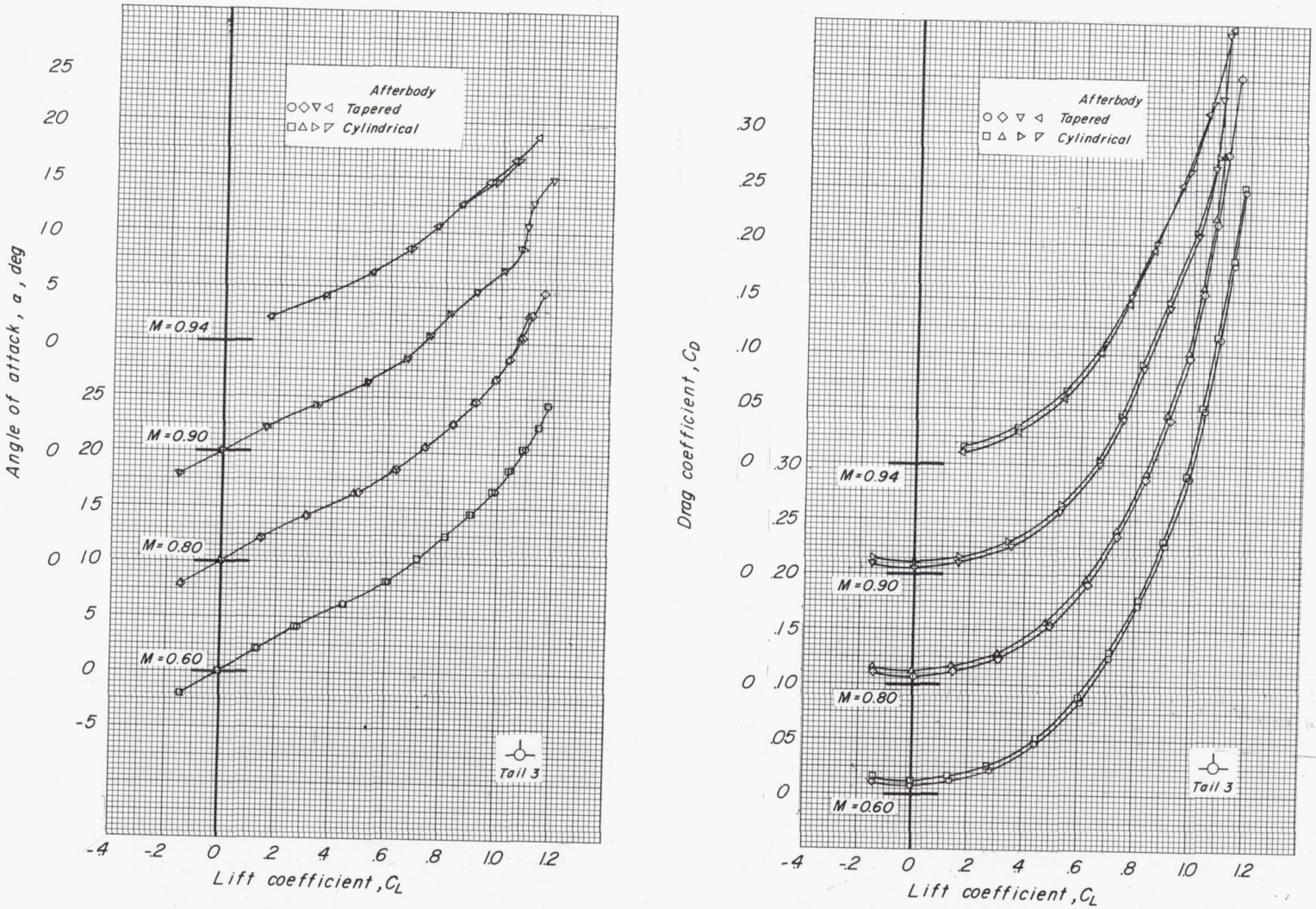

Figure 8.- Aerodynamic characteristics in pitch for the model with tail 3. $i_t = 0^\circ$.

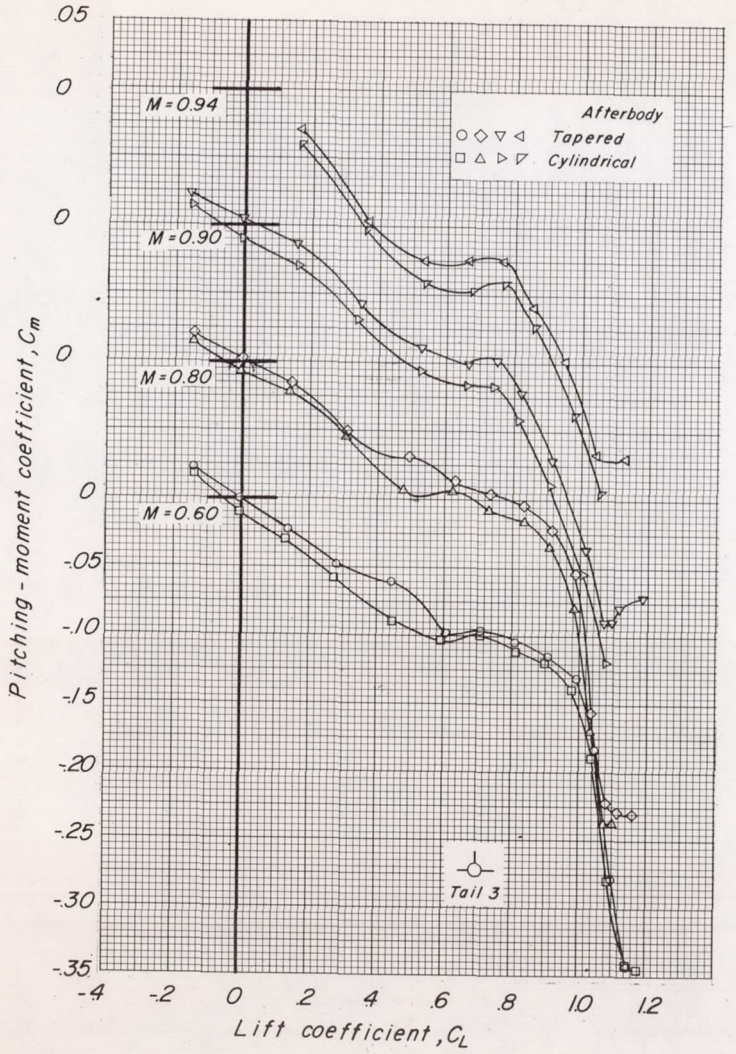

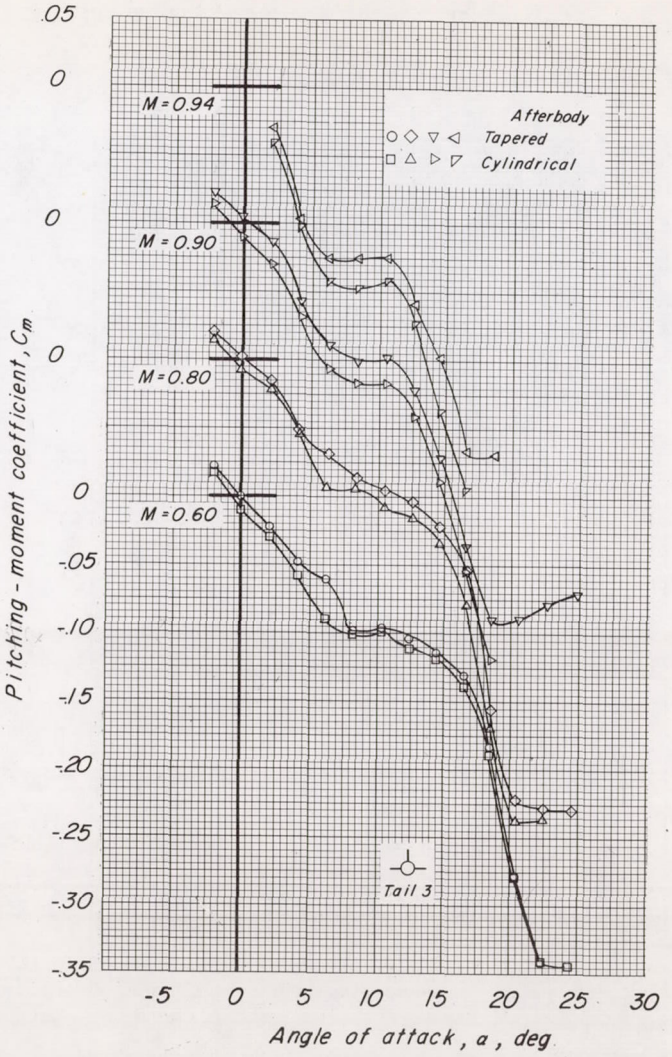

Figure 8.- Concluded.

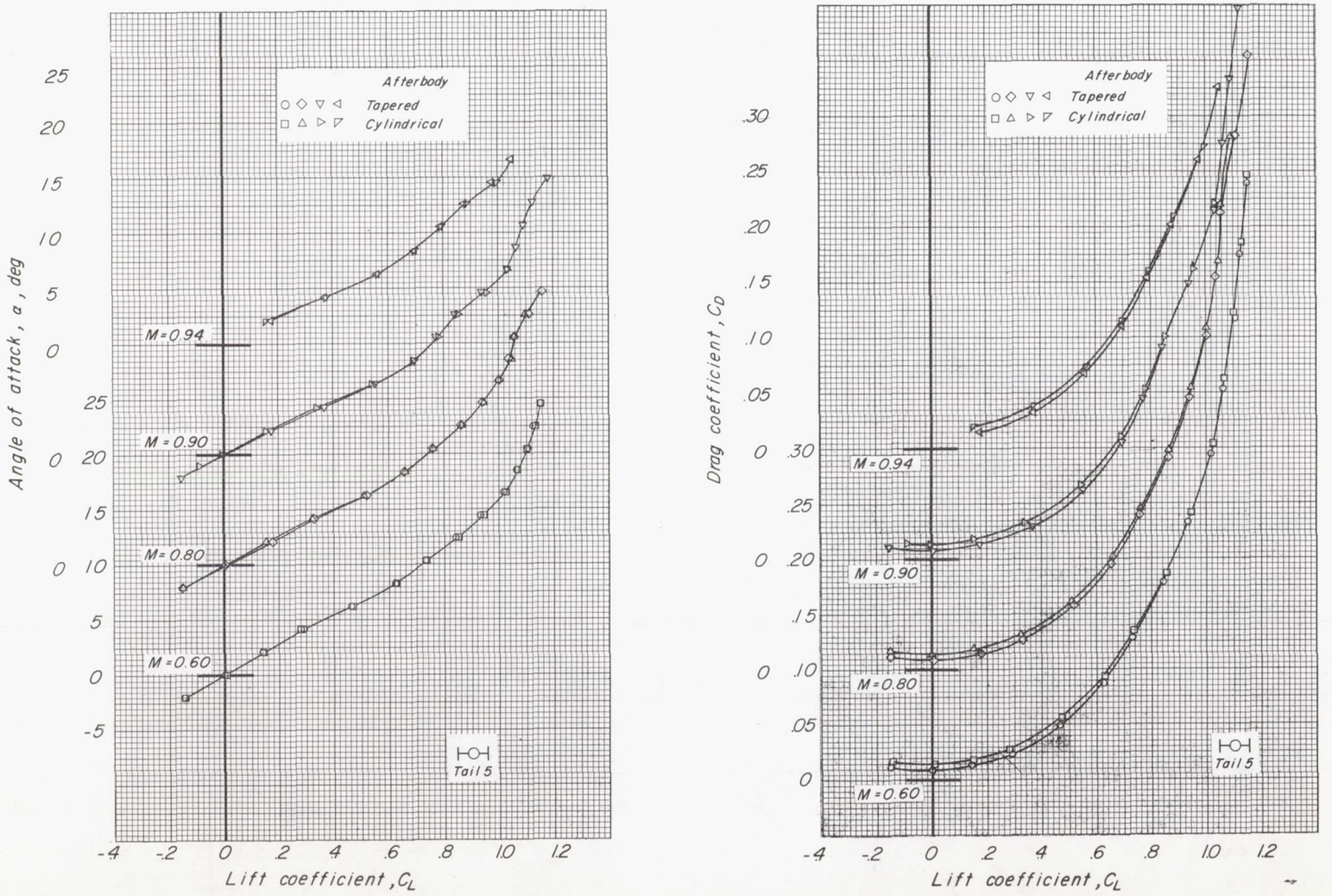

Figure 9.- Aerodynamic characteristics in pitch for the model with tail 5. $i_t = 0^o$.

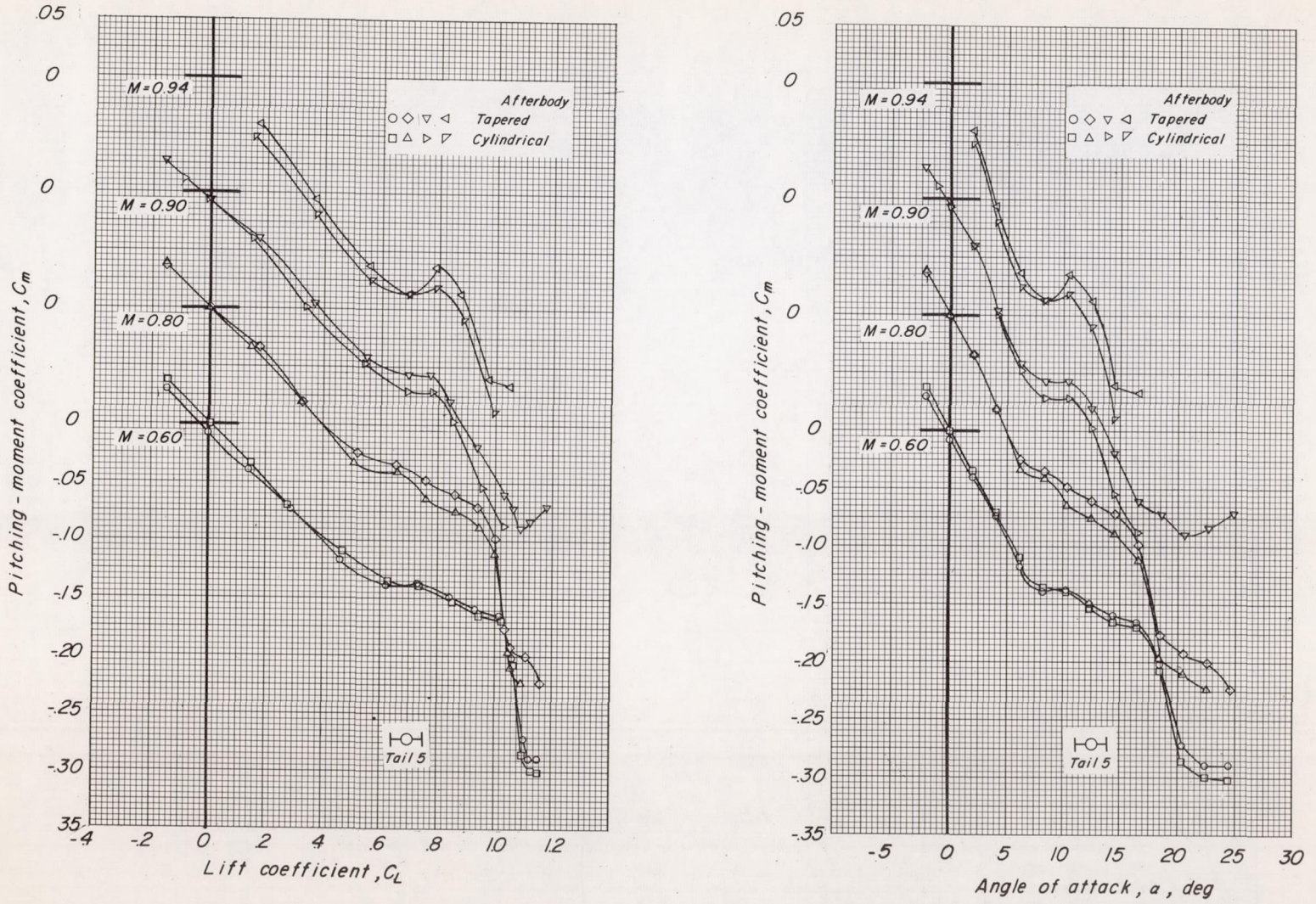

Figure 9.- Concluded.

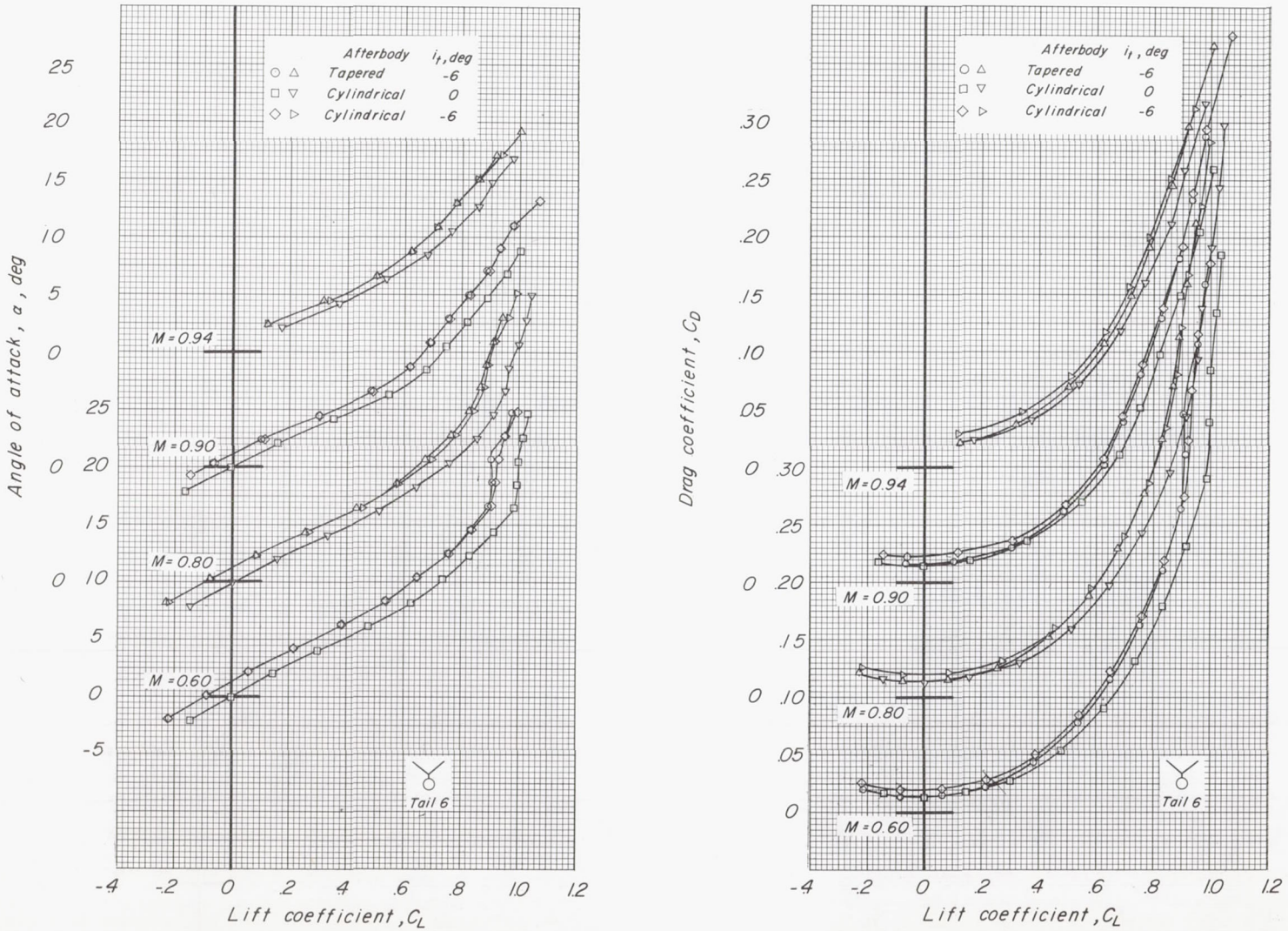

Figure 10.- Aerodynamic characteristics in pitch for the model with tail 6.

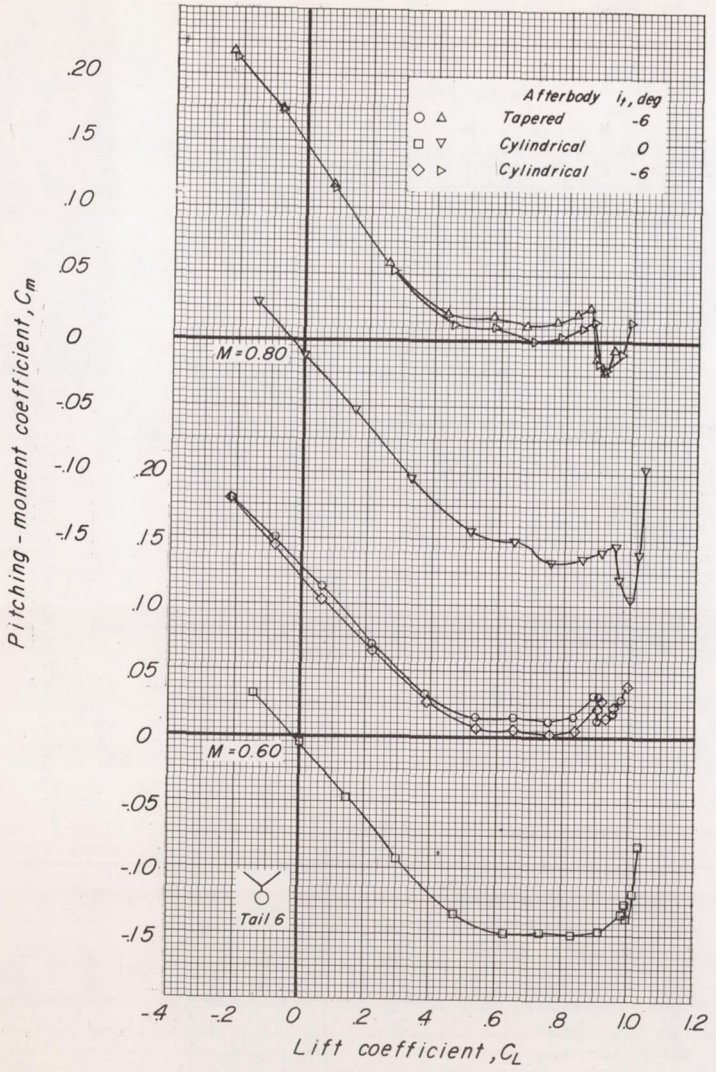

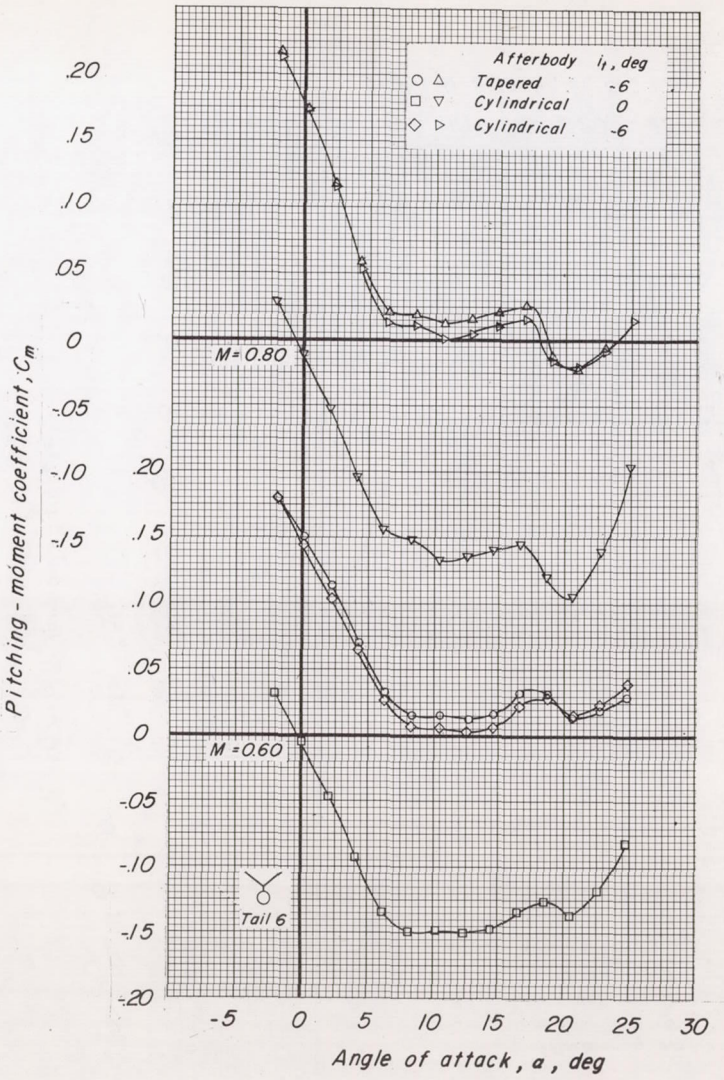

Figure 10.- Continued.

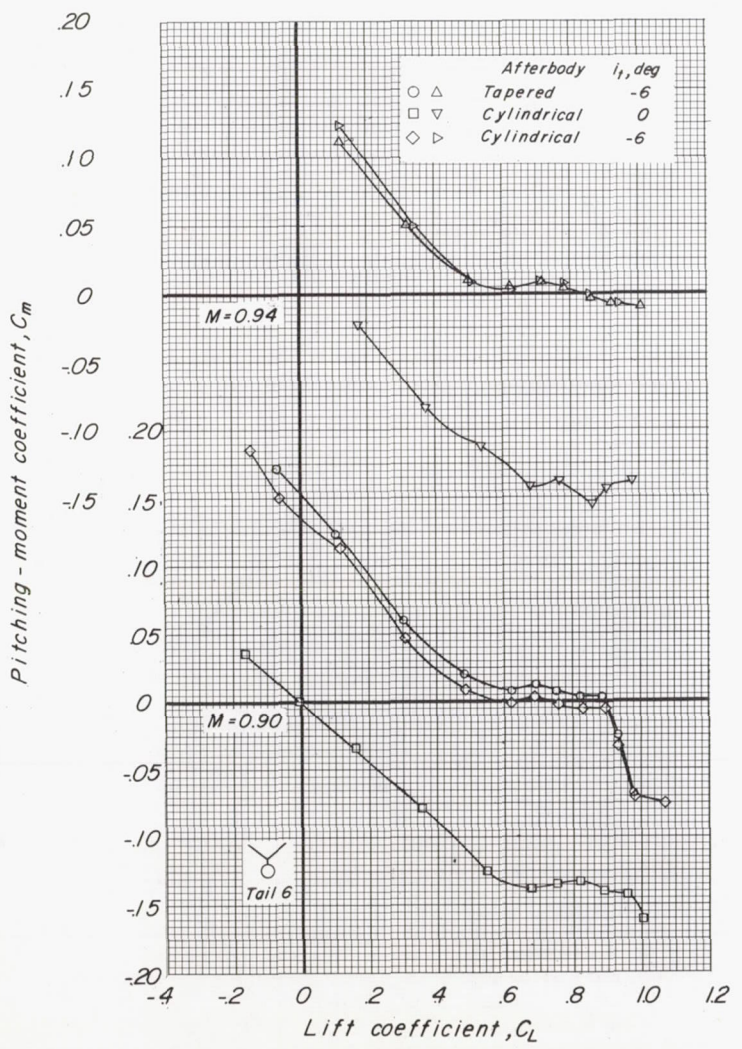

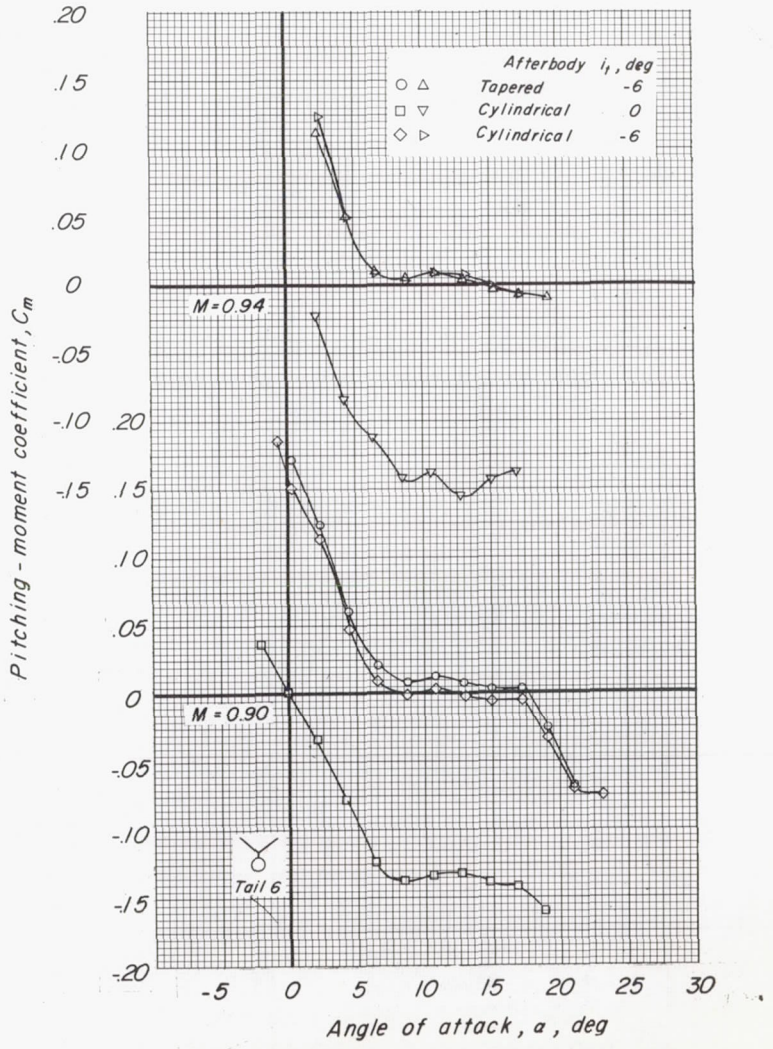

Figure 10.- Concluded.

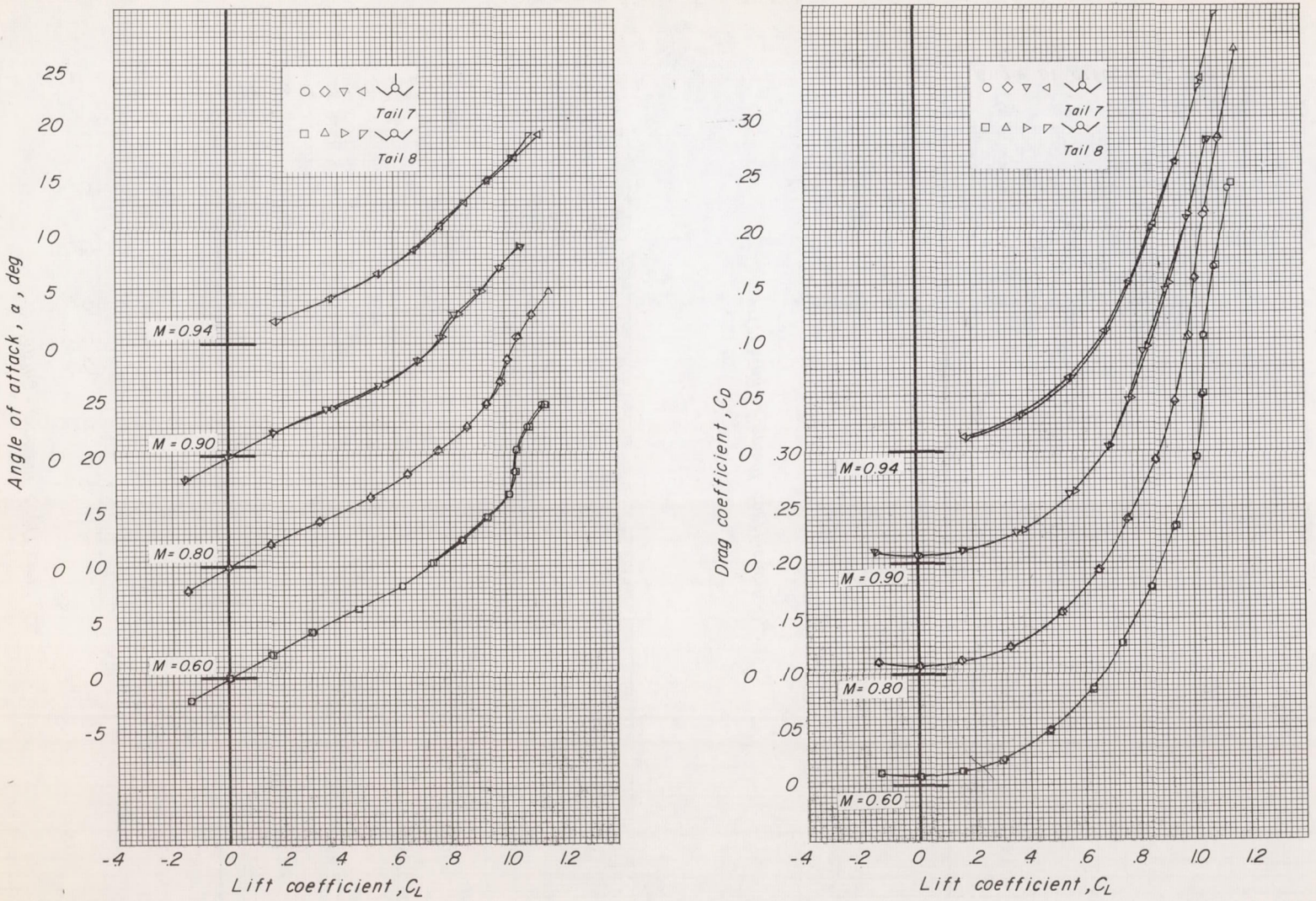

Figure 11.- Aerodynamic characteristics in pitch for the model with tail 7 and tail 8. $i_t = 0^\circ$. Tapered afterbody.

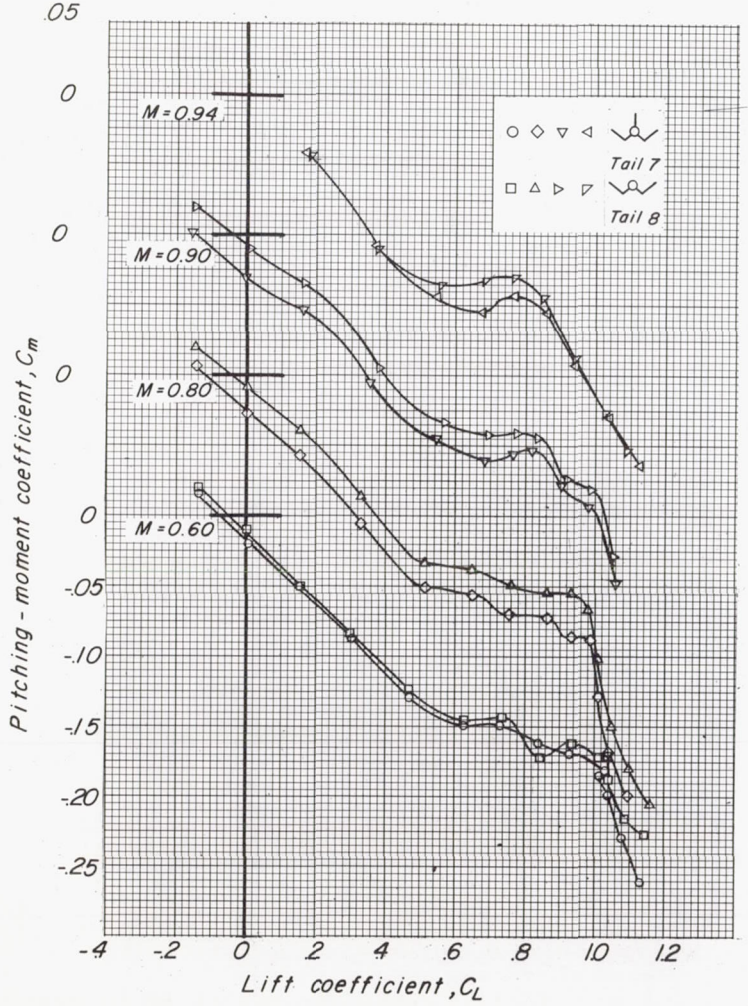

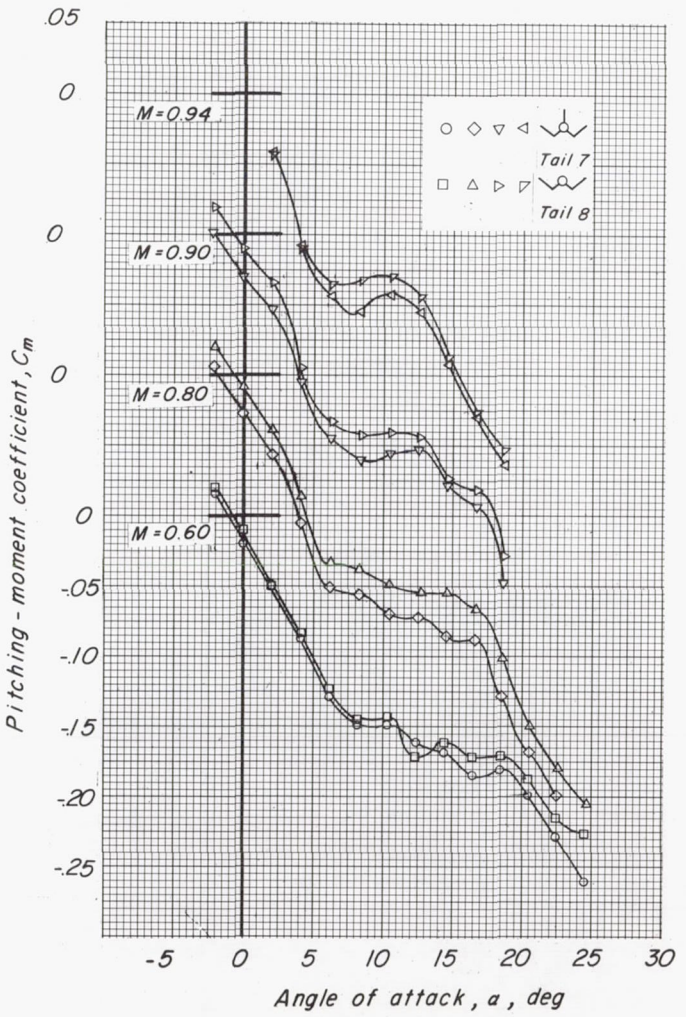

Figure 11.- Concluded.

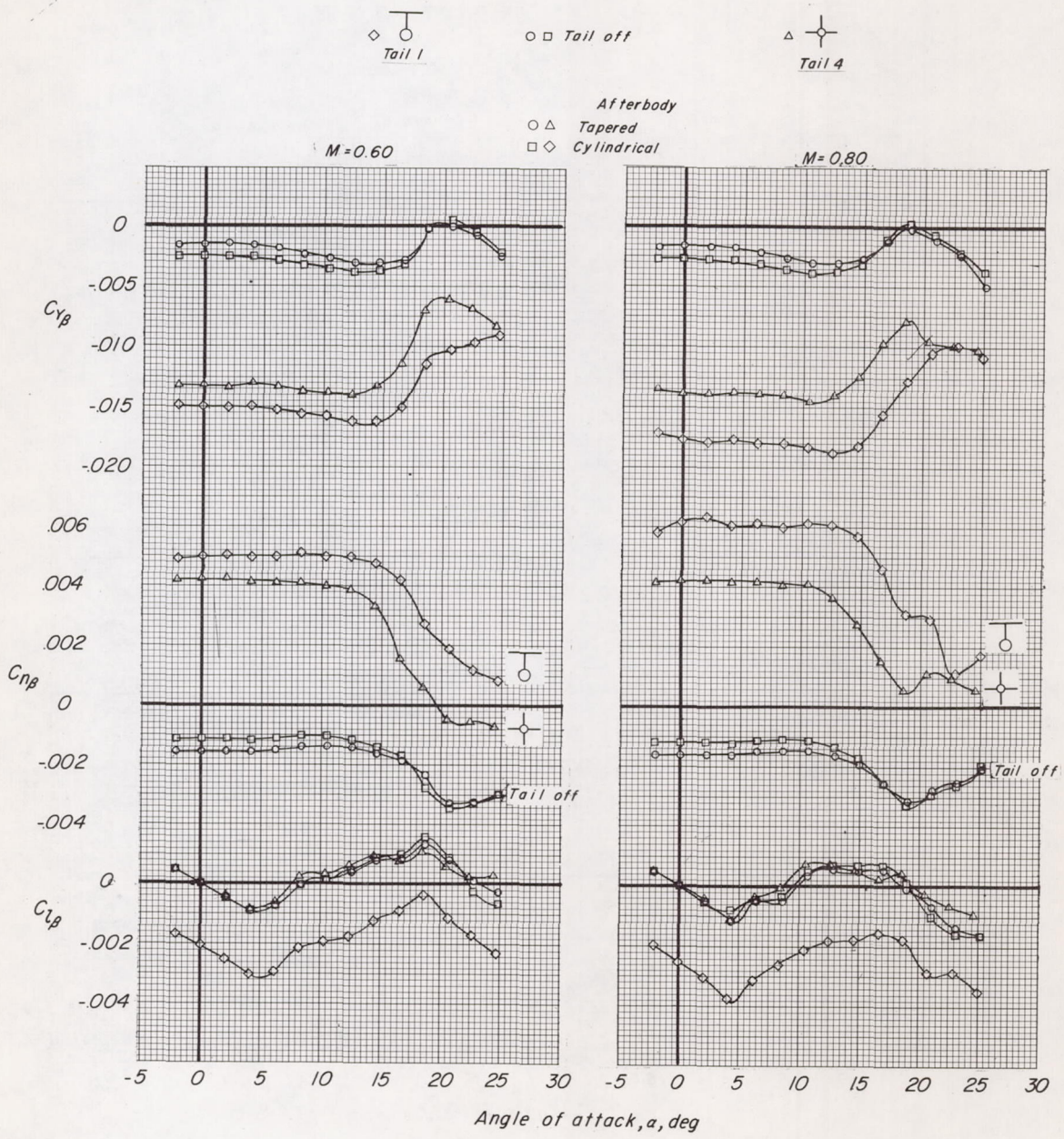

Figure 12.- Lateral stability derivatives of the model with tail 1, tail 4, and without a tail. $i_t = 0^\circ$ for tail-on configurations.

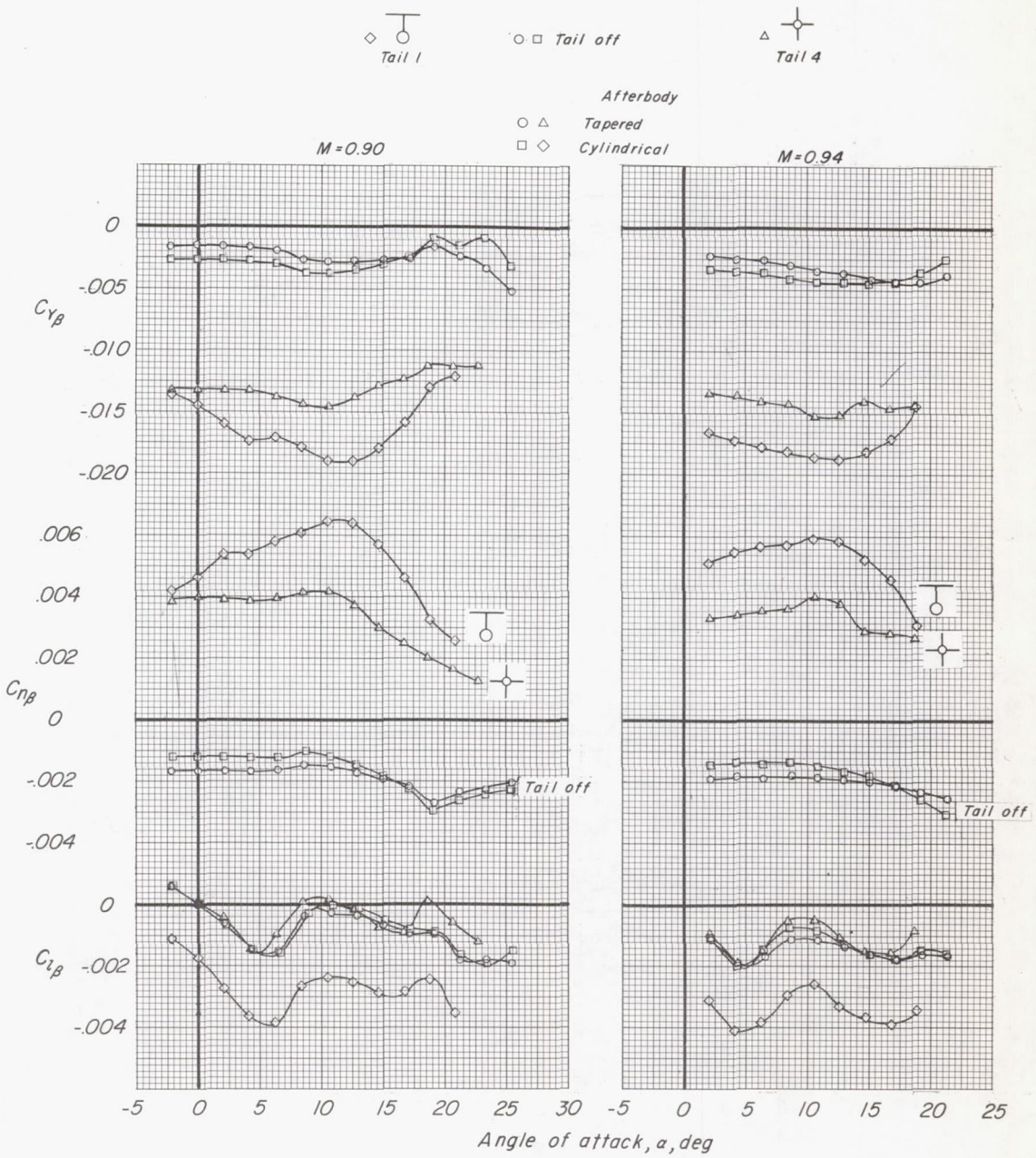

Figure 12.- Concluded.

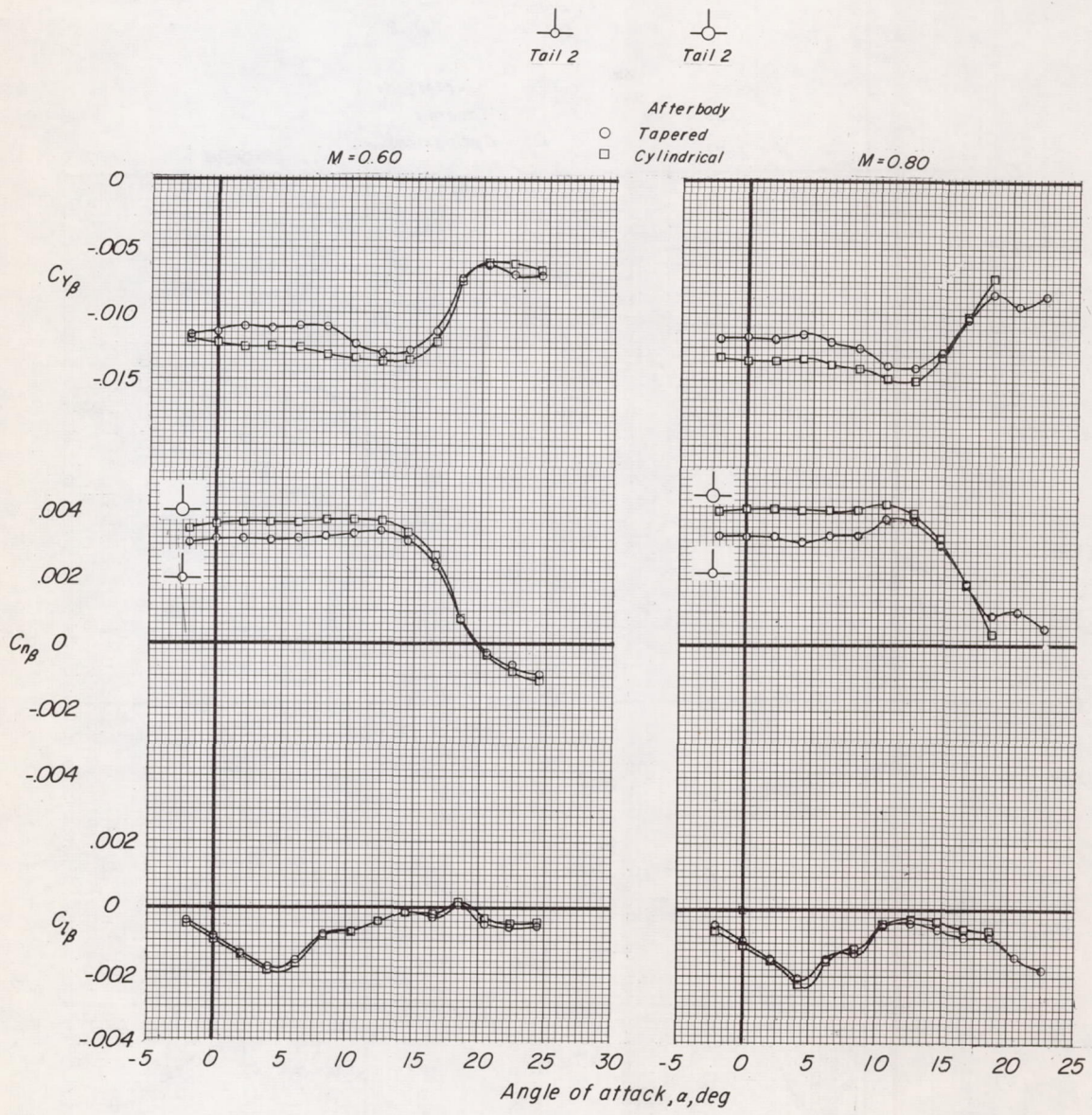

Figure 13.- Lateral stability derivatives of the model with tail 2. $i_t = 0^\circ$.

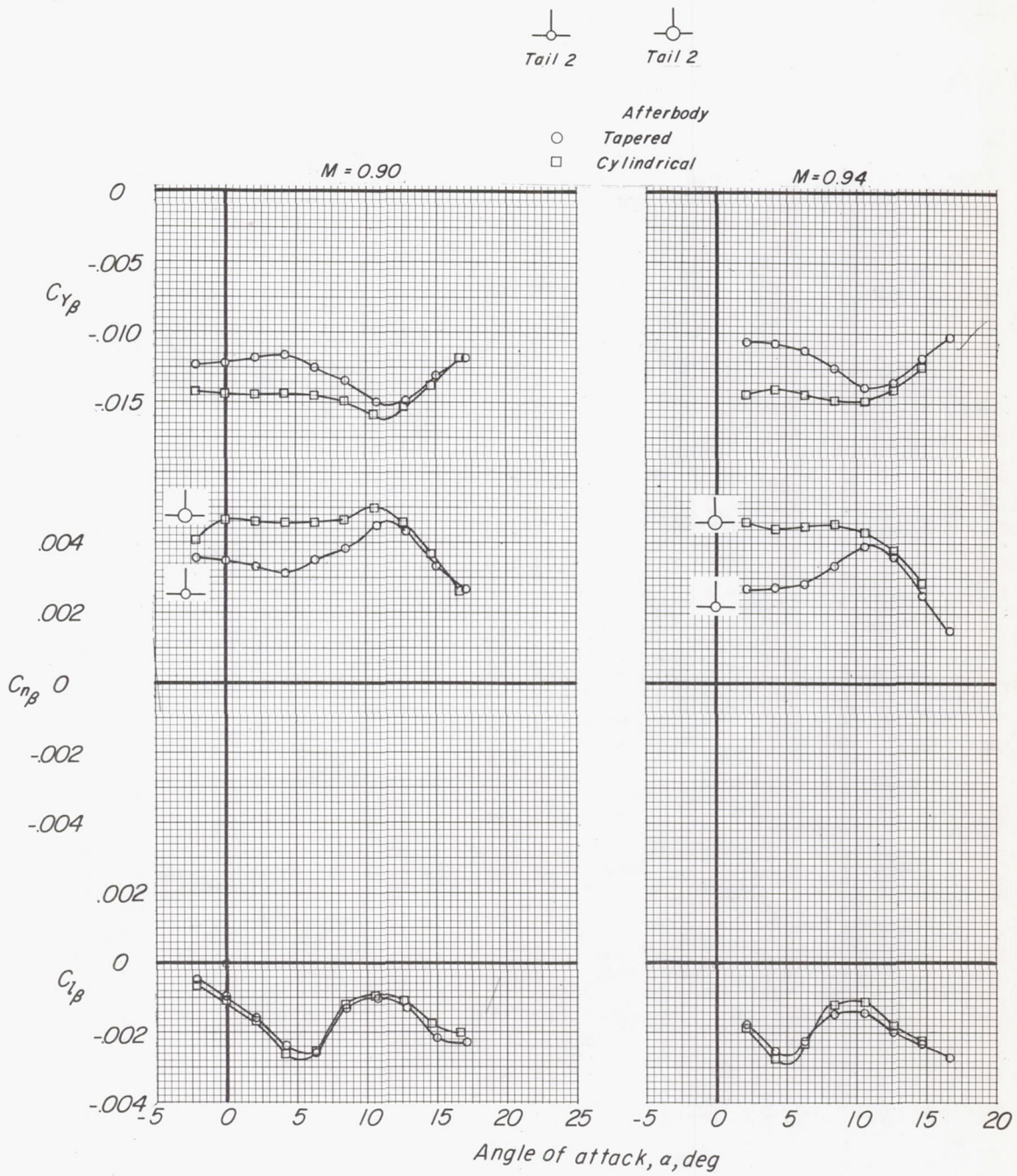

Figure 13.- Concluded.

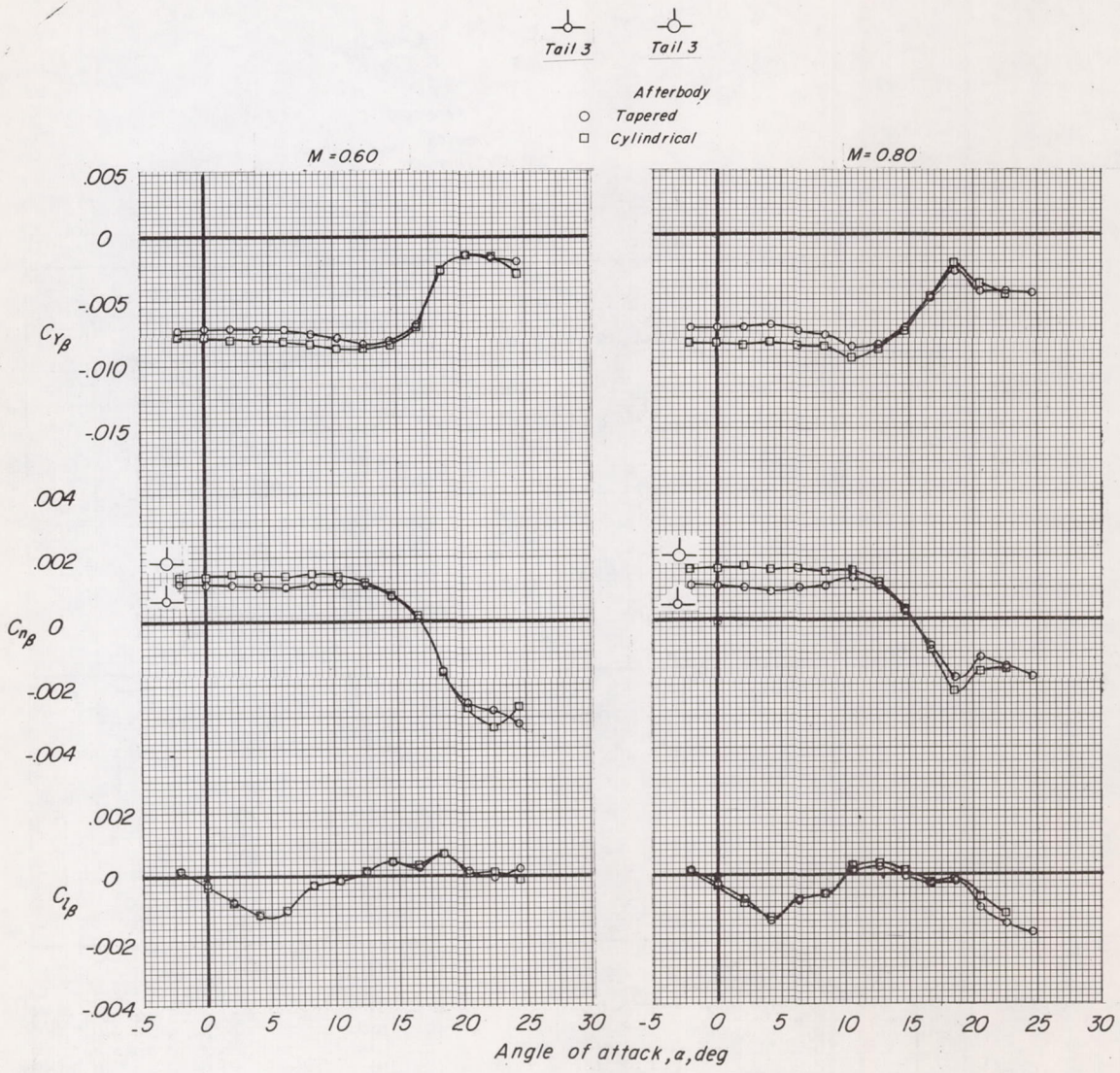

Figure 14.- Lateral stability derivatives of the model with tail 3. $i_t = 0^\circ$.

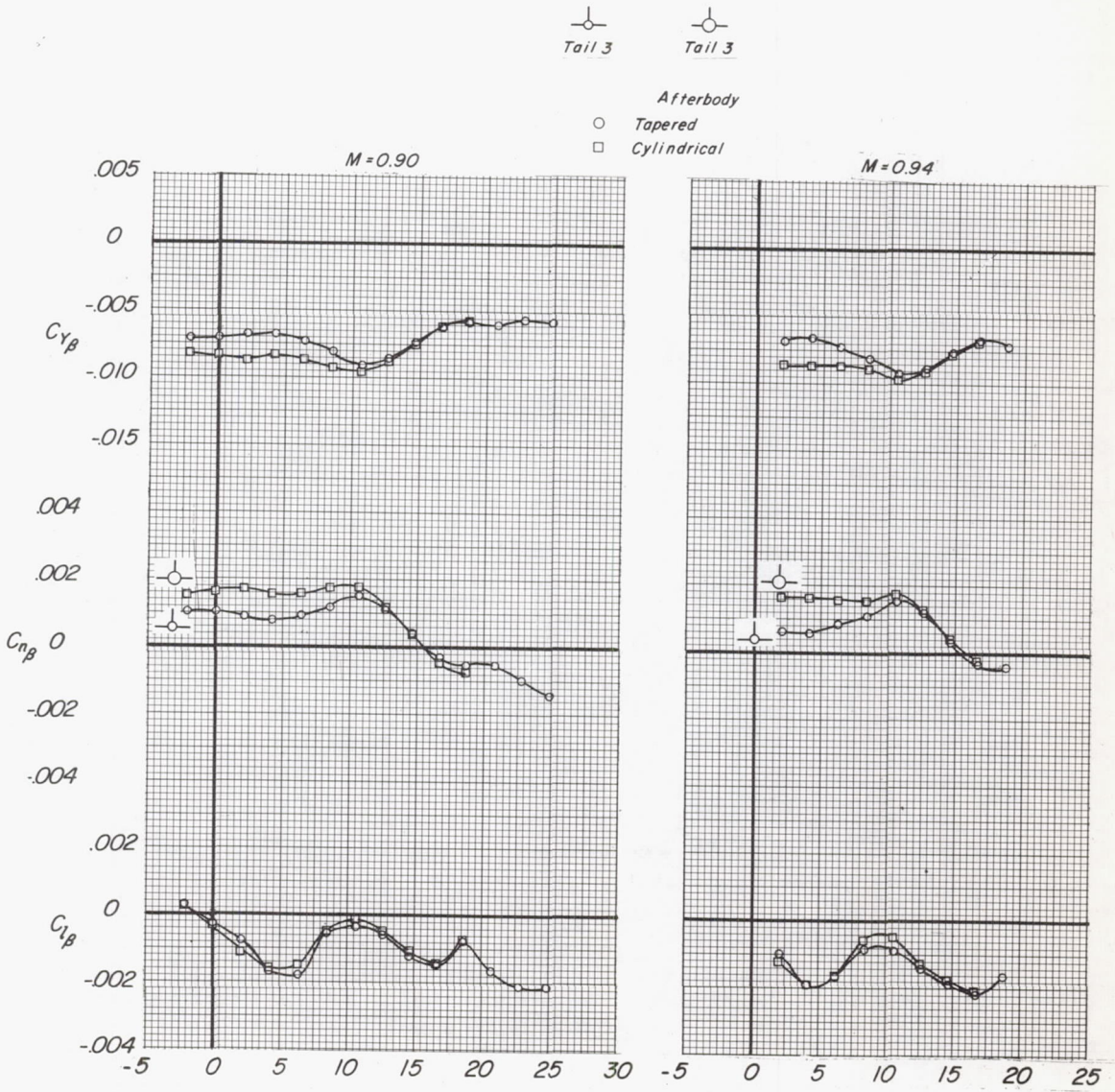

Figure 14.- Concluded.

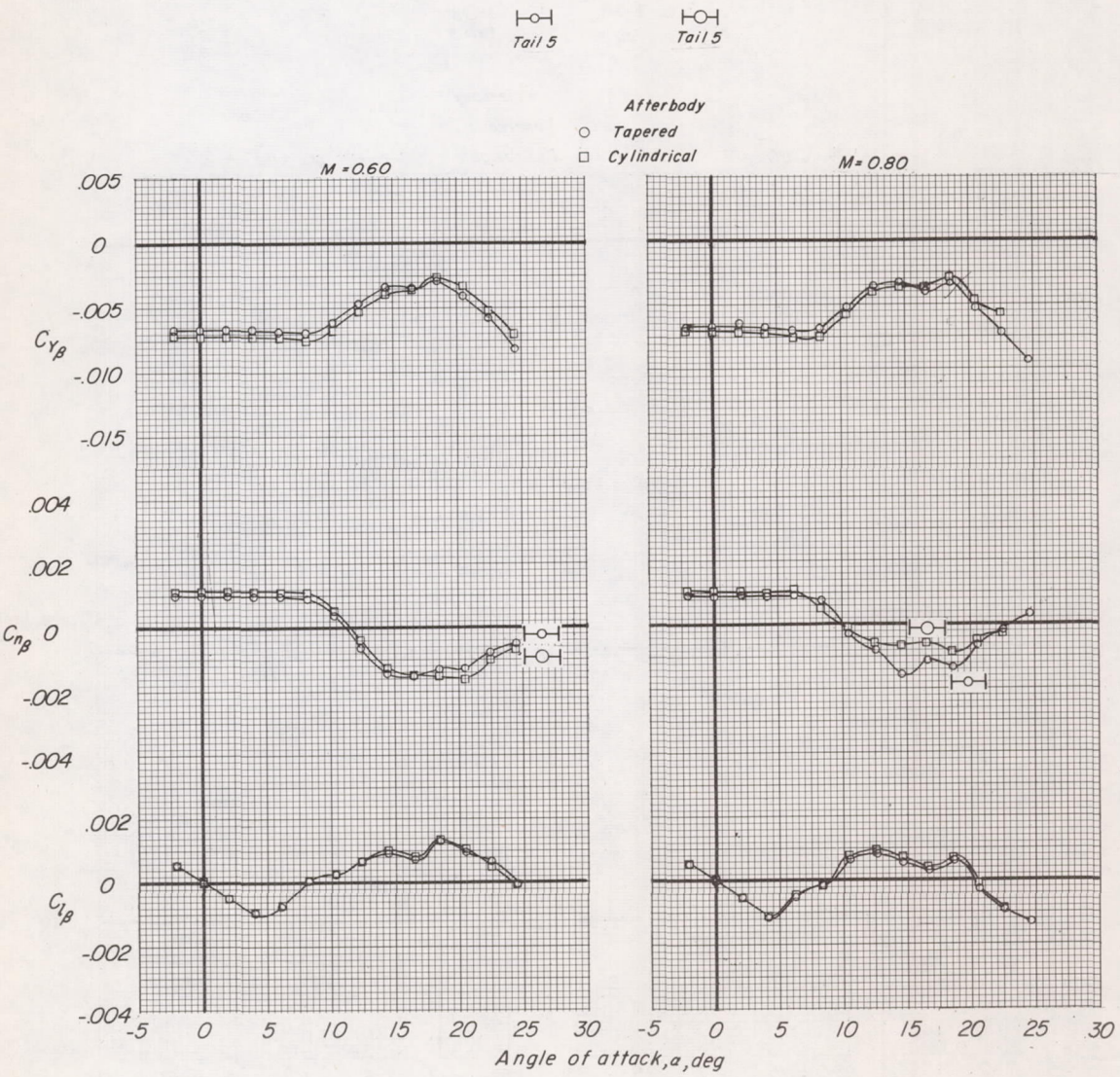

Figure 15.- Lateral stability derivatives of the model with tail 5. $i_t = 0^\circ$.

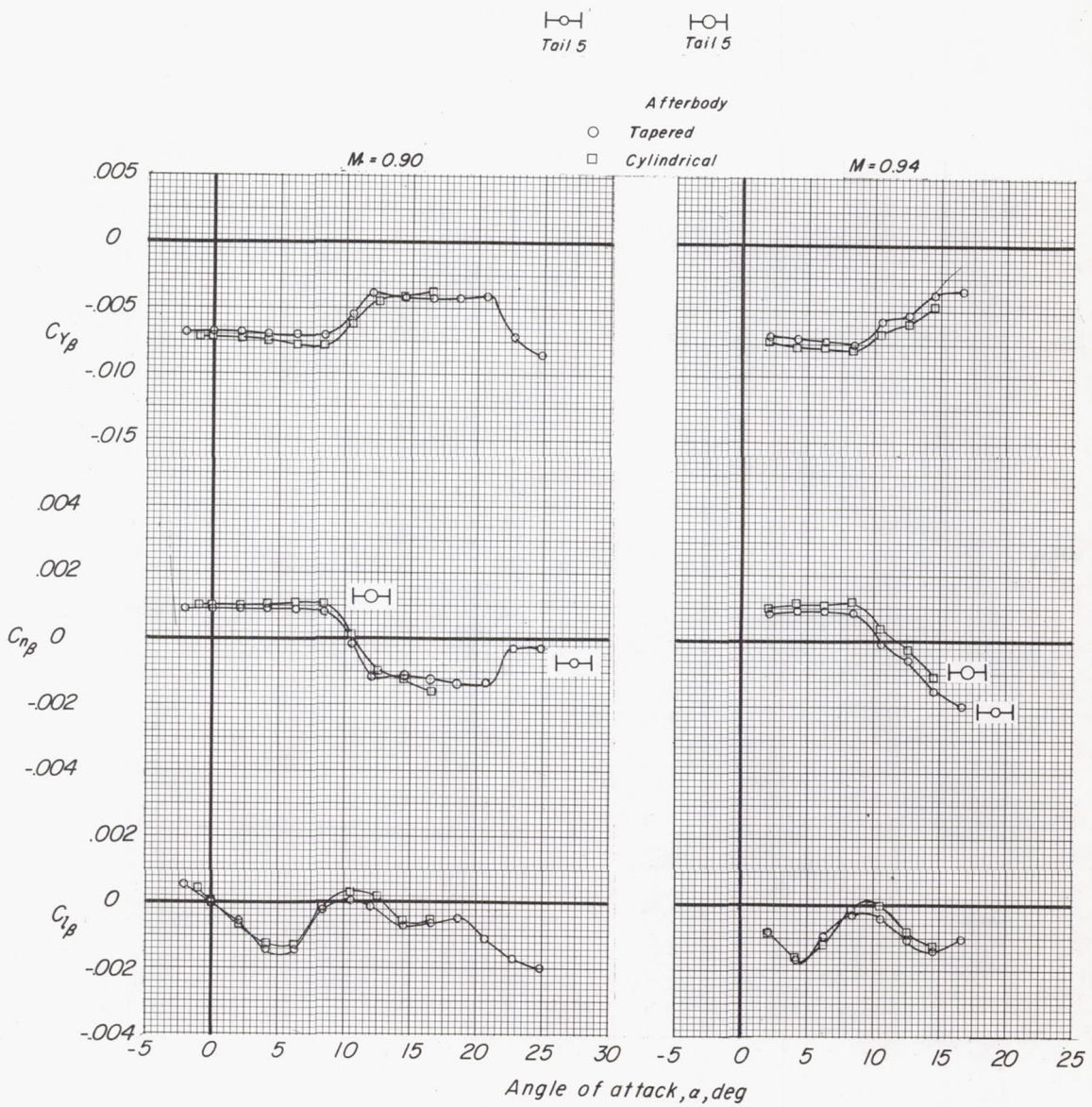

Figure 15.- Concluded.

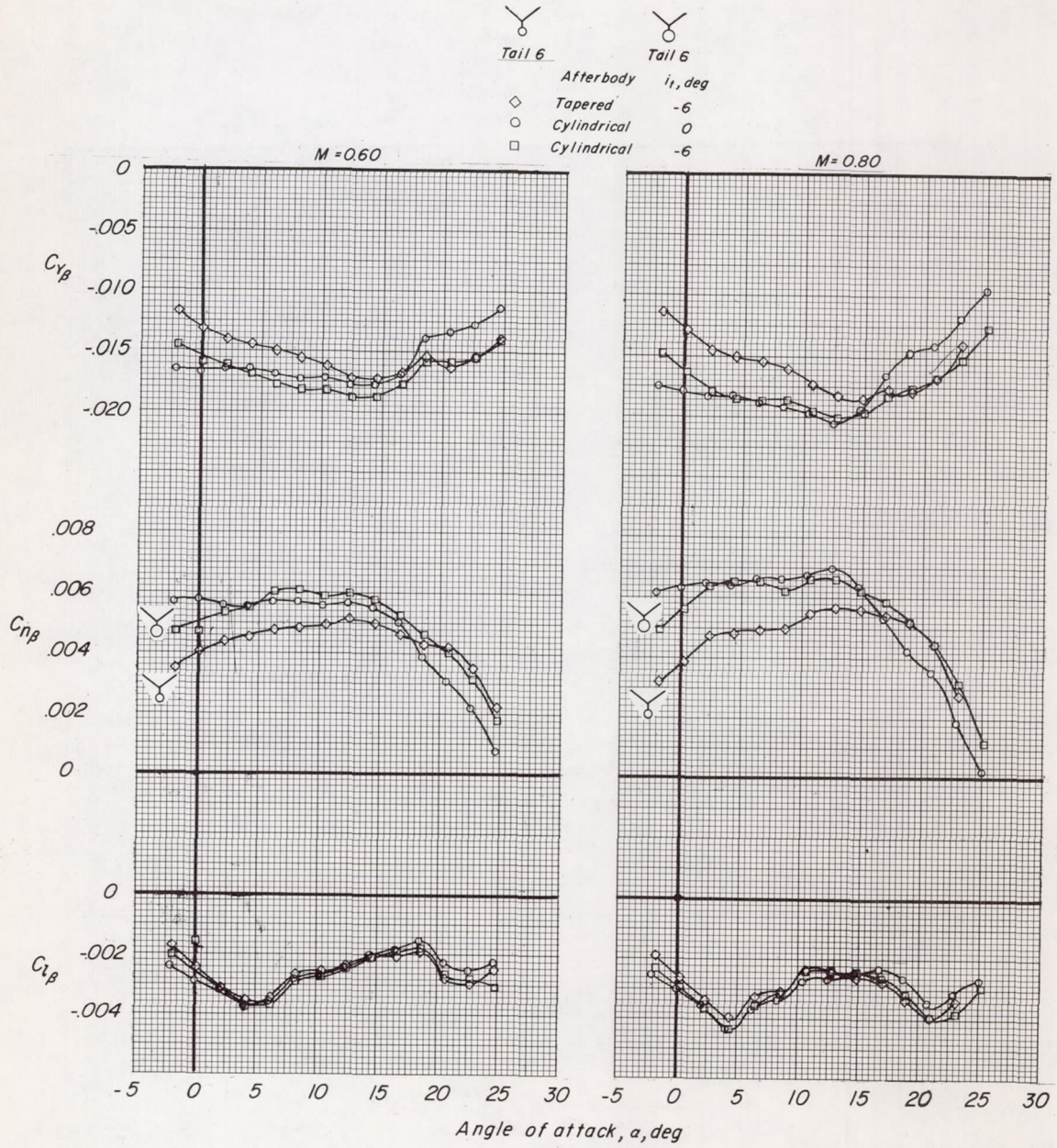

Figure 16.- Lateral stability derivatives of the model with tail 6.

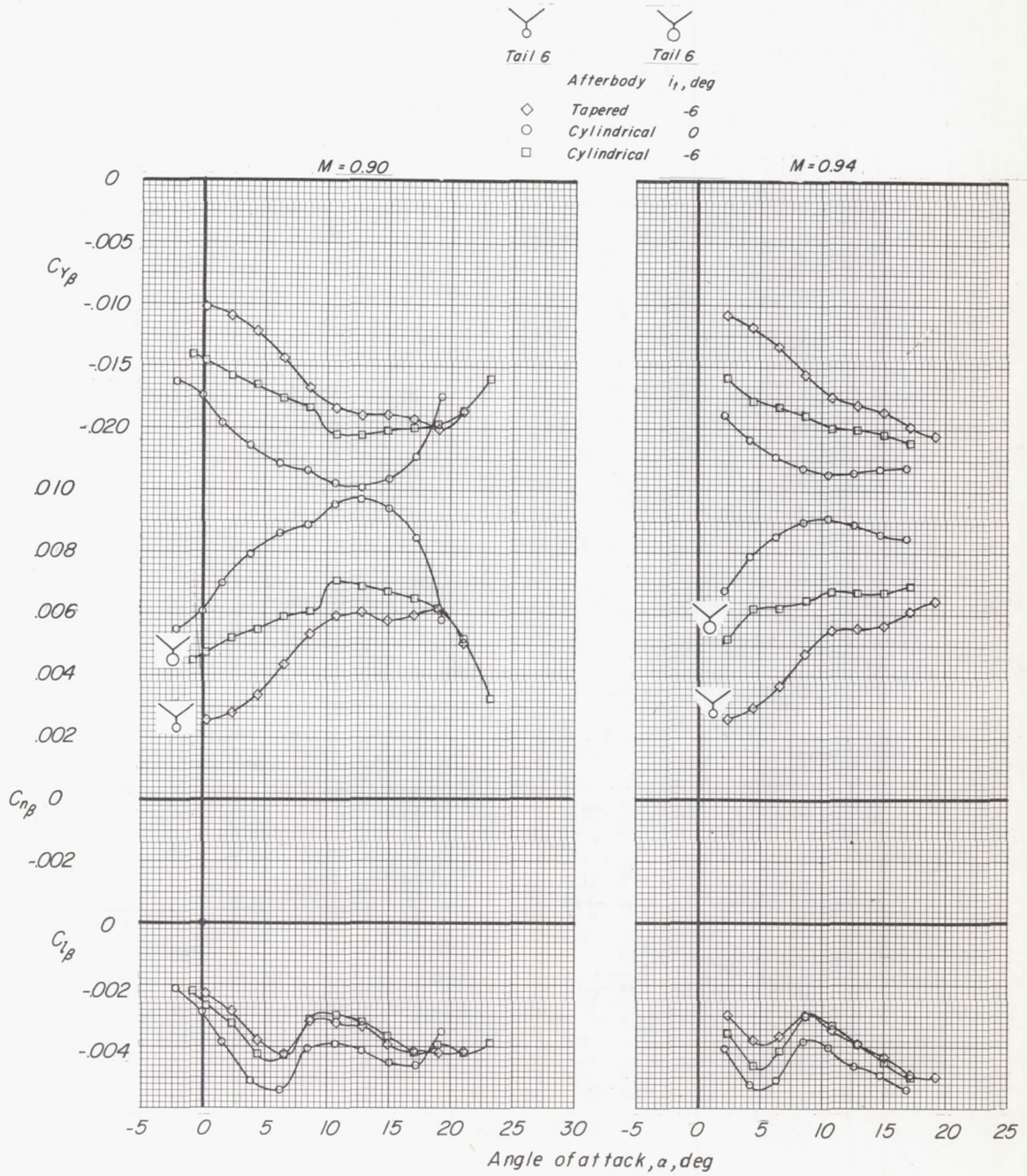

Figure 16.- Concluded.

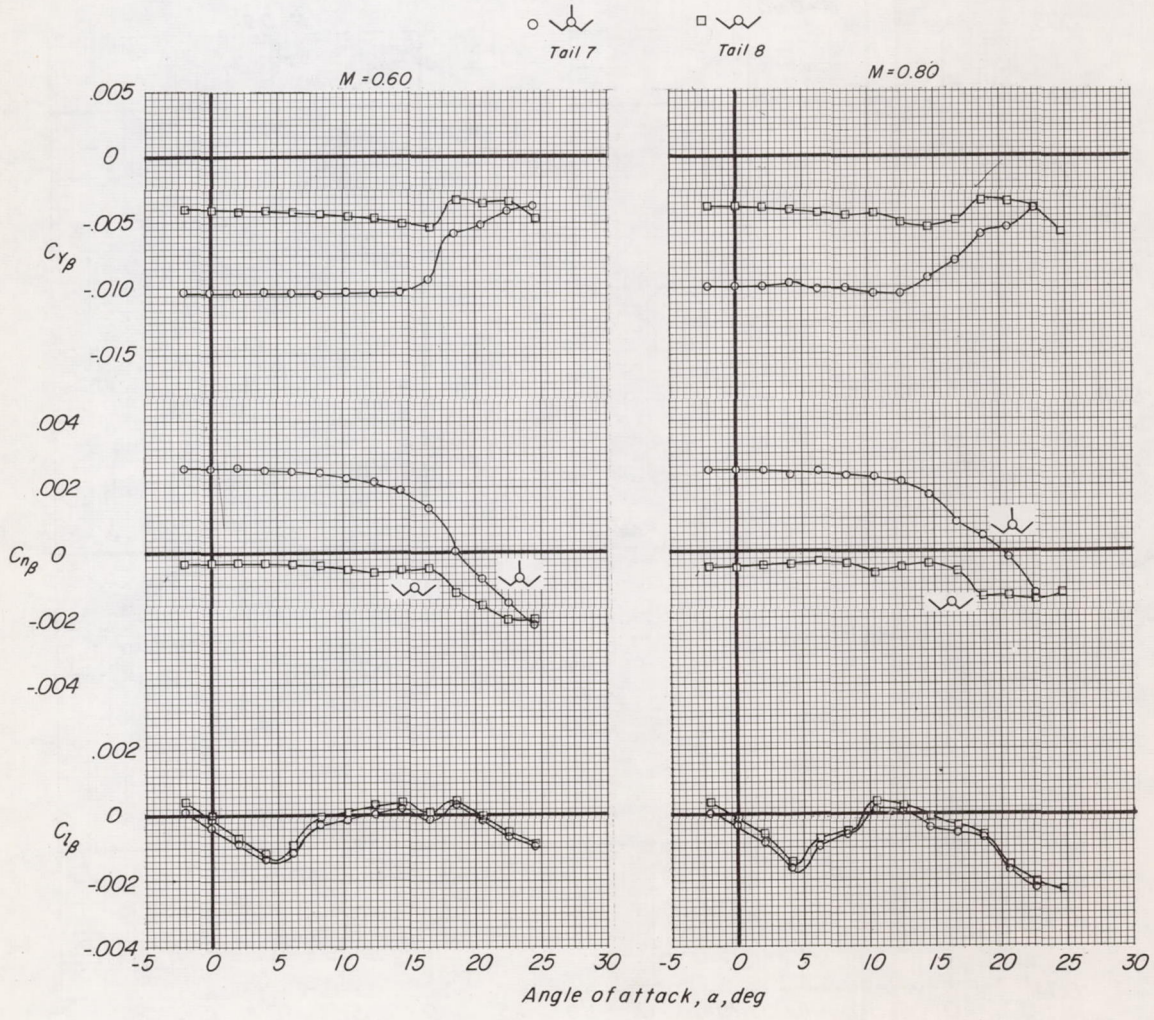

Figure 17.- Lateral stability derivatives of the model with tail 7 and tail 8. $i_t = 0^o$.

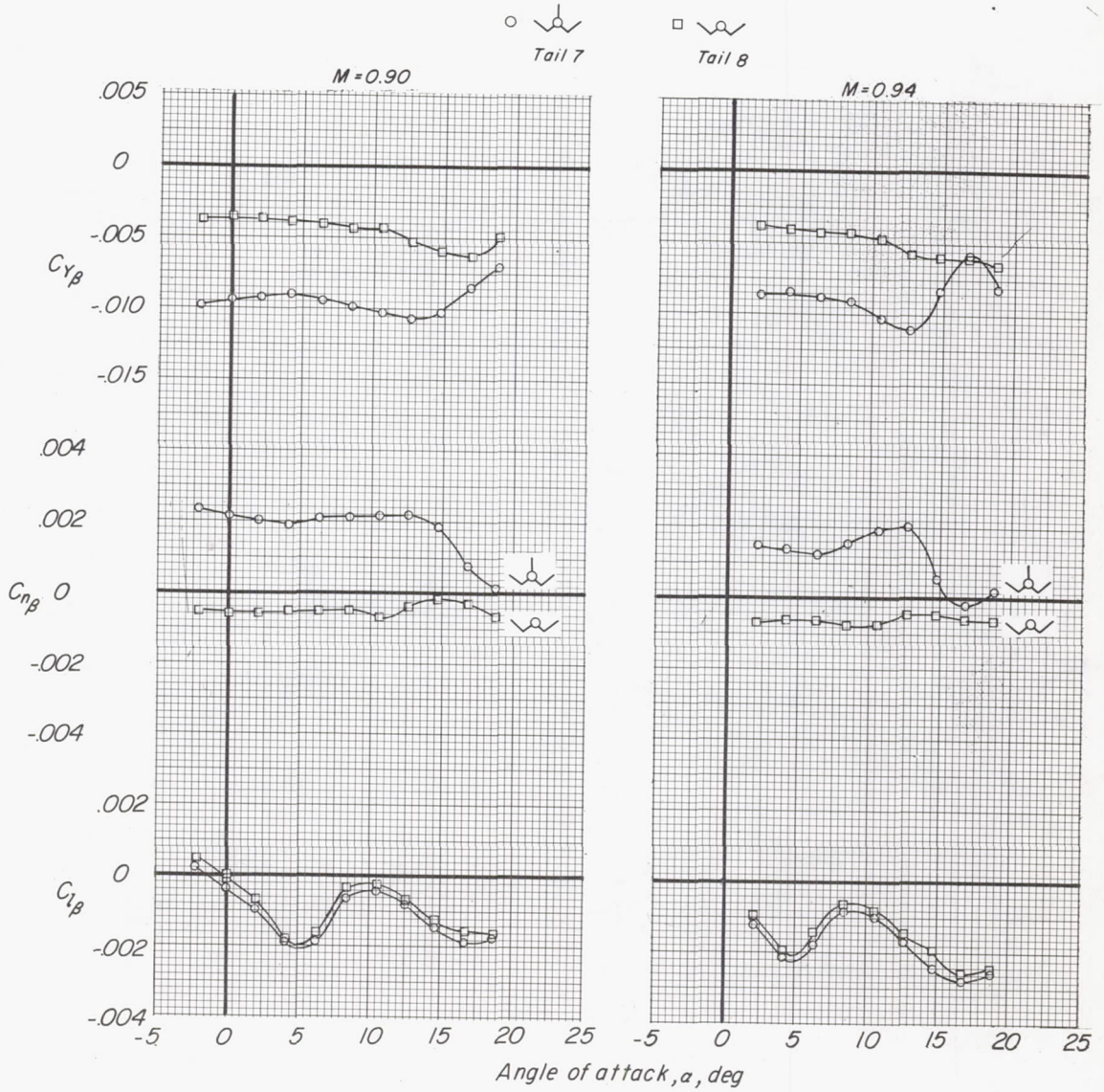

Figure 17.- Concluded.

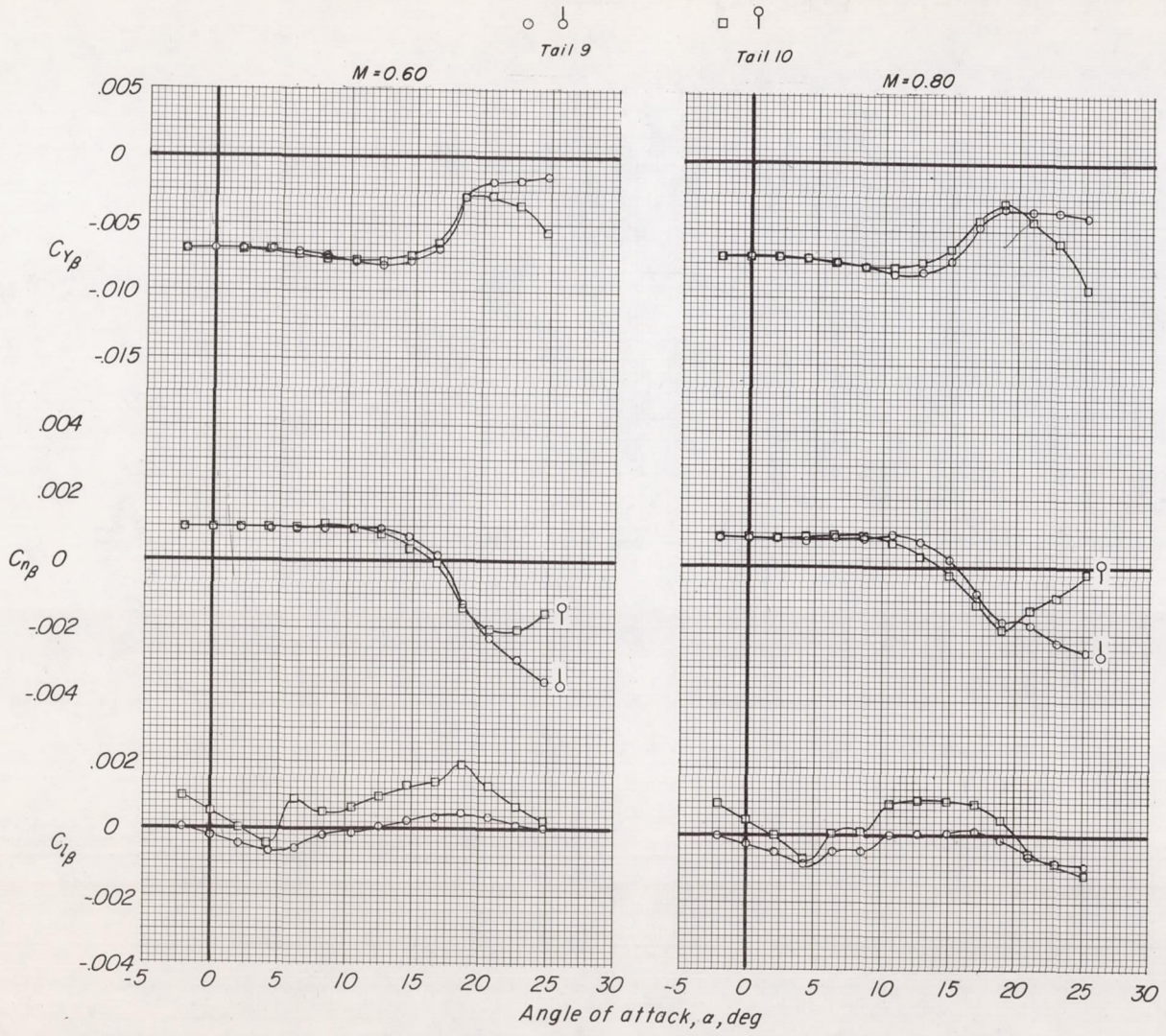

Figure 18.- Lateral stability derivatives of the model with tail 9 and tail 10. Tapered afterbody.

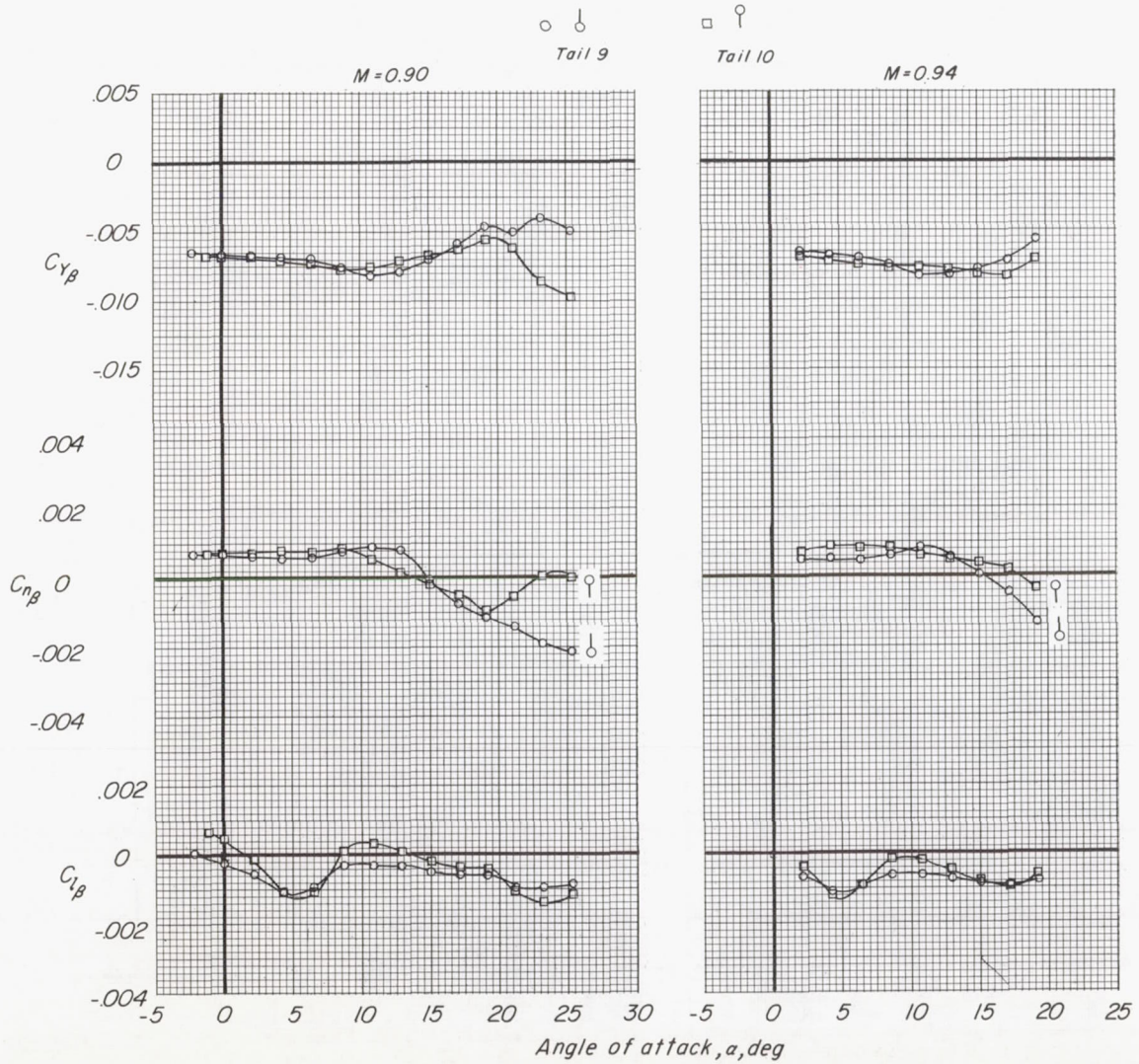

Figure 18.- Concluded.

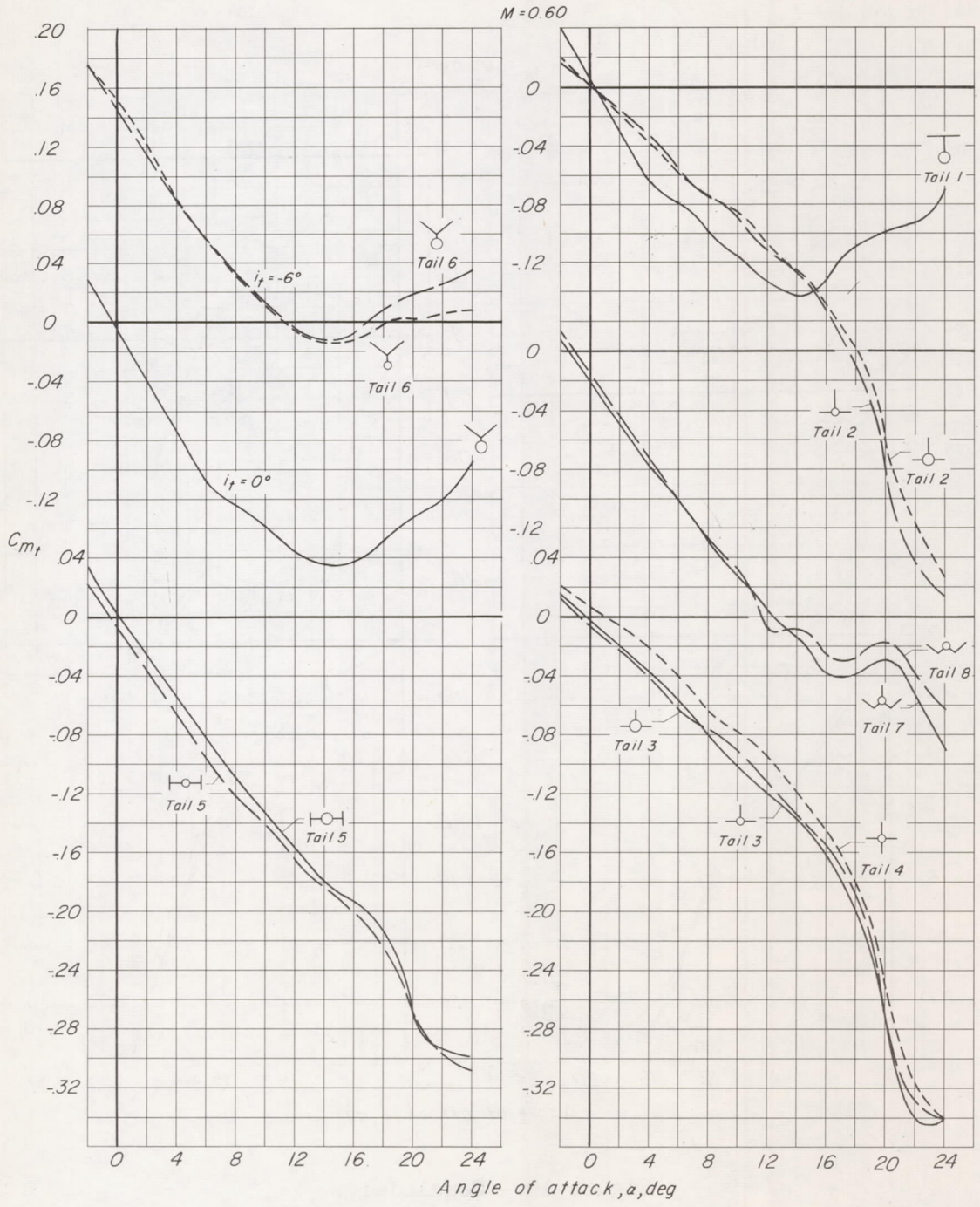

Figure 19.- Tail contribution to pitching moments of the model with the various tail configurations. $i_t = 0^\circ$ except as indicated otherwise.

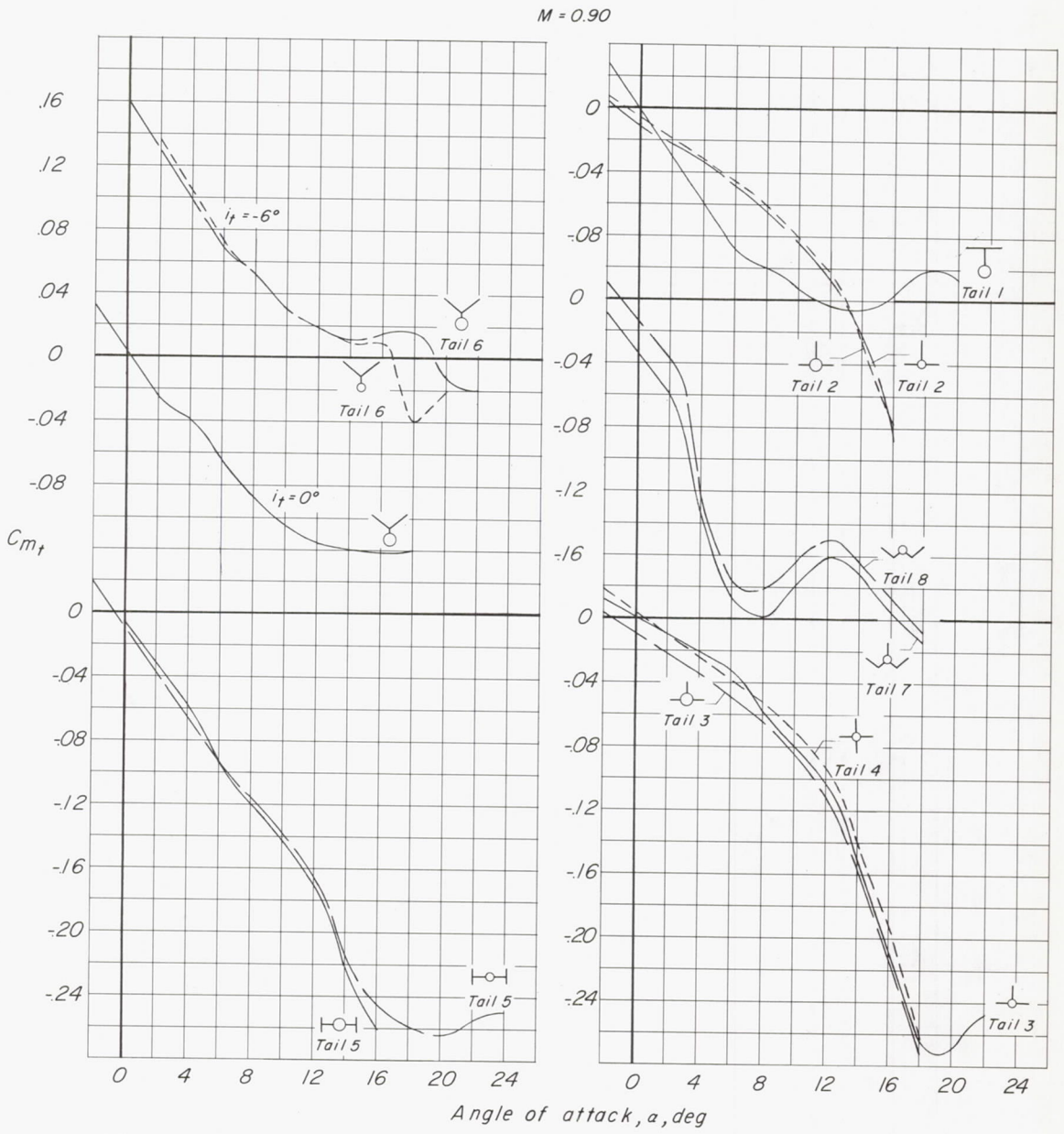

Figure 19.- Concluded.

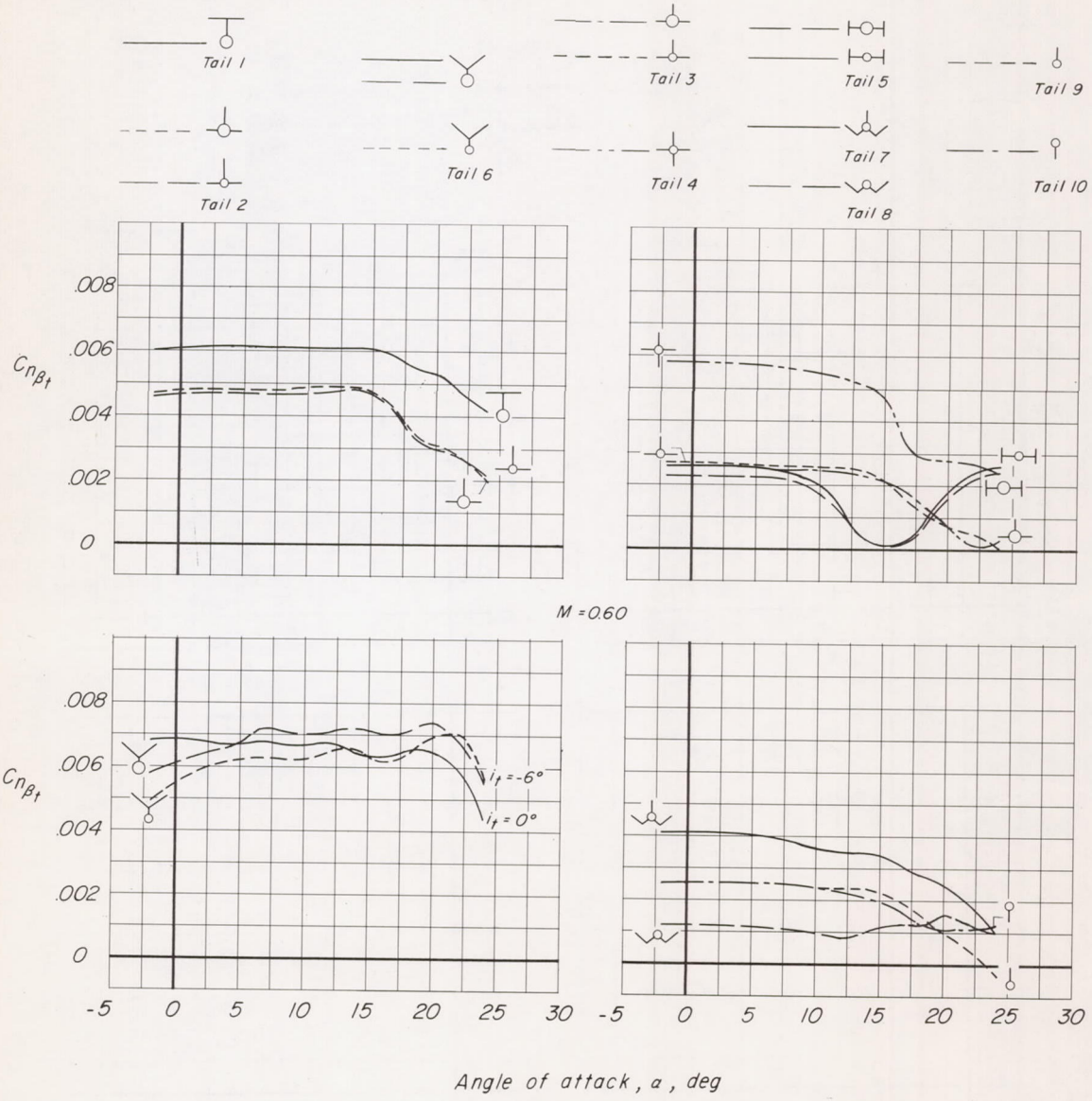

Figure 20.- Tail contribution to directional stability of the model with the various tail configurations. $i_t = 0^\circ$ except as indicated otherwise.

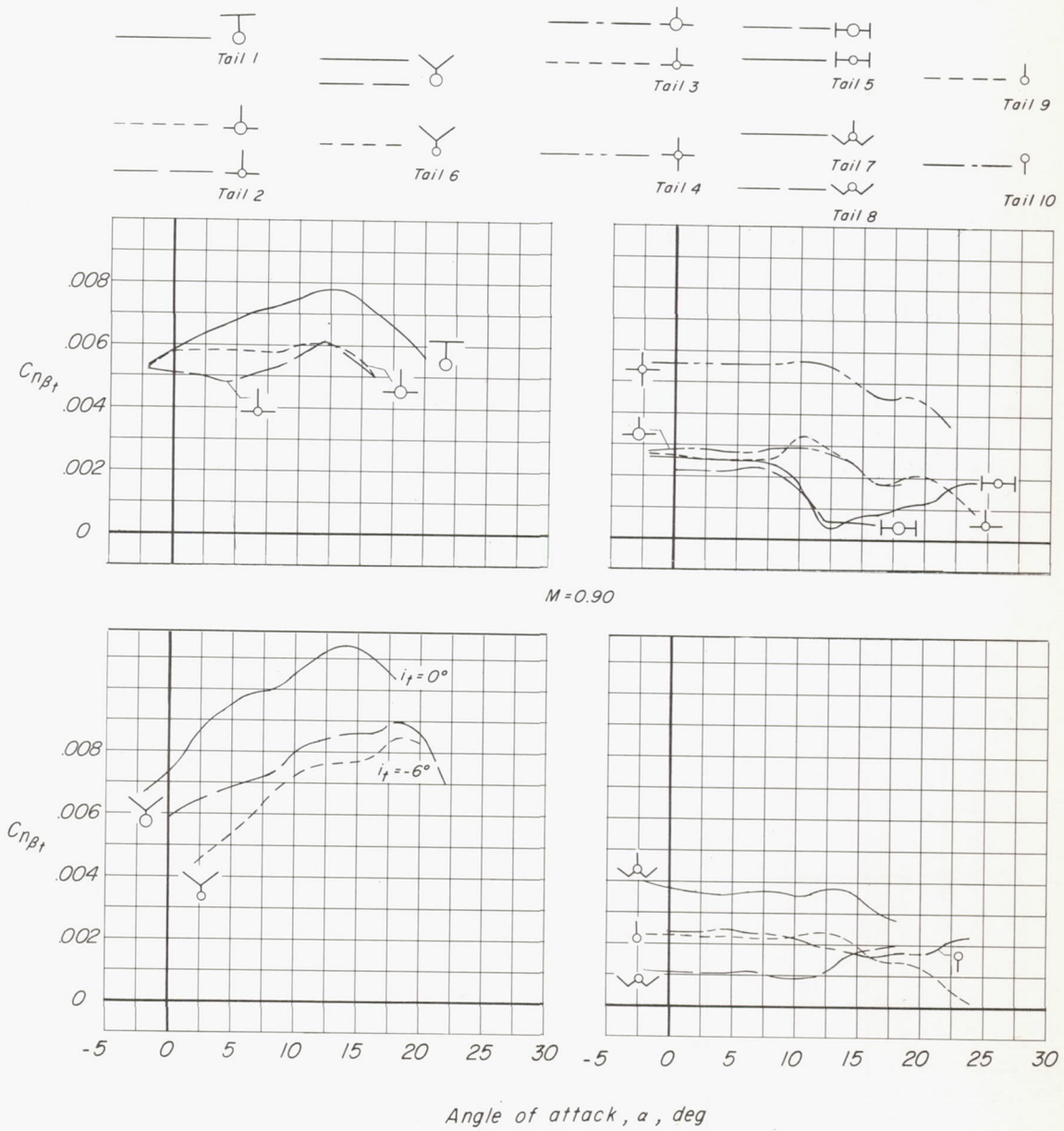

Figure 20.- Concluded.

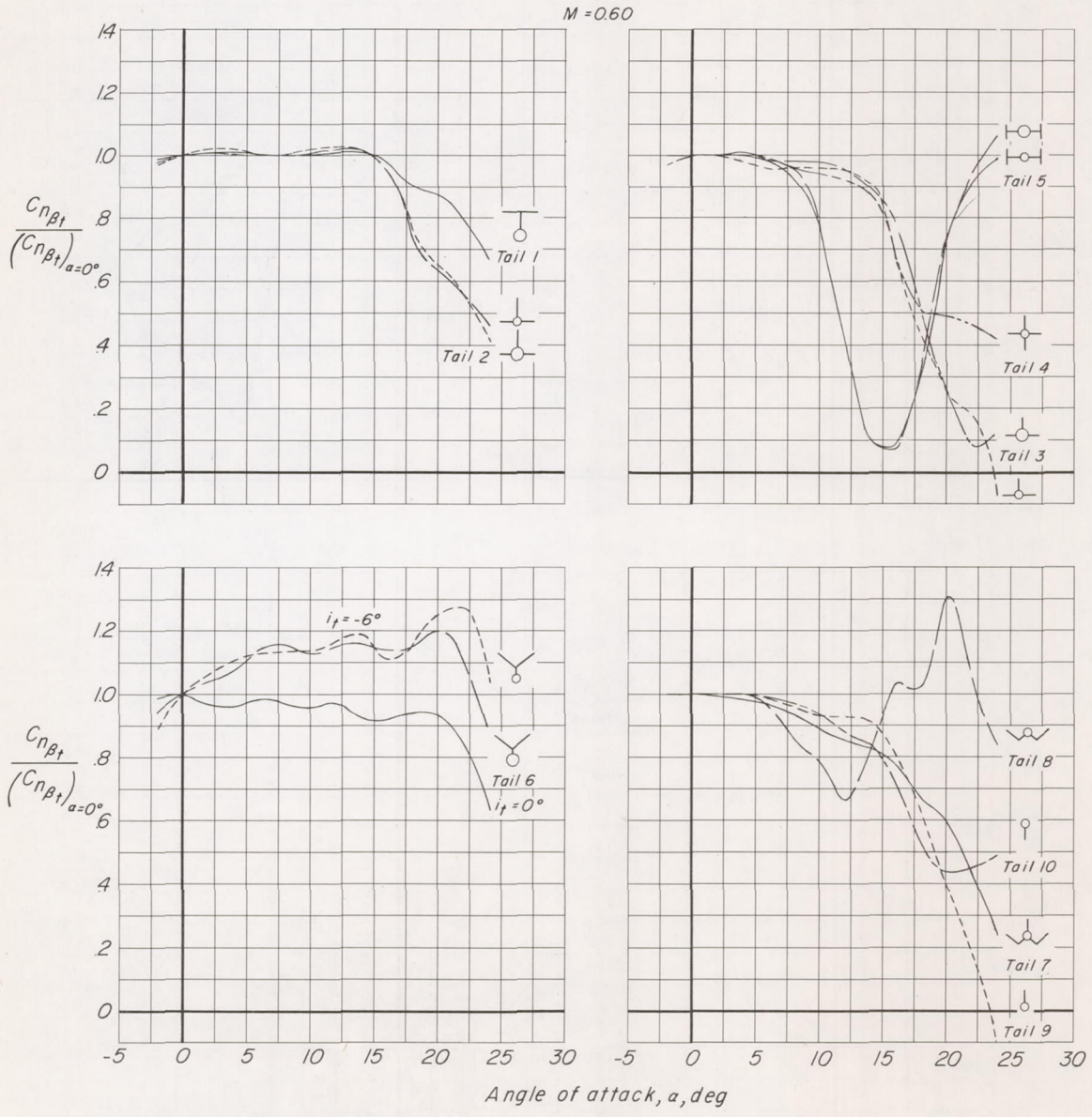

Figure 21.- Effects of angle of attack on the tail contribution to directional stability of the model with the various tail configurations. $i_t = 0^o$ except as indicated otherwise.

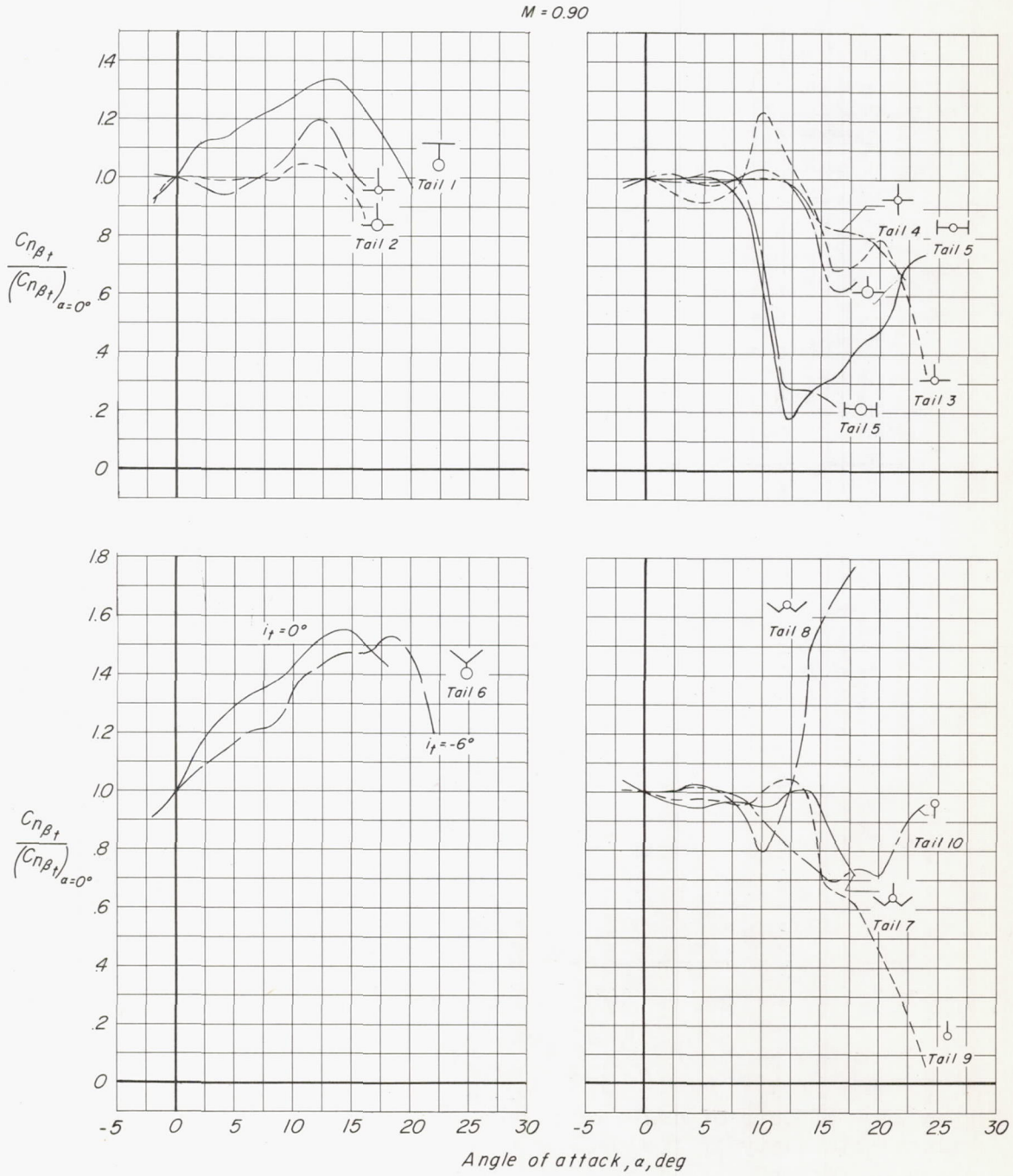

Figure 21.- Concluded.

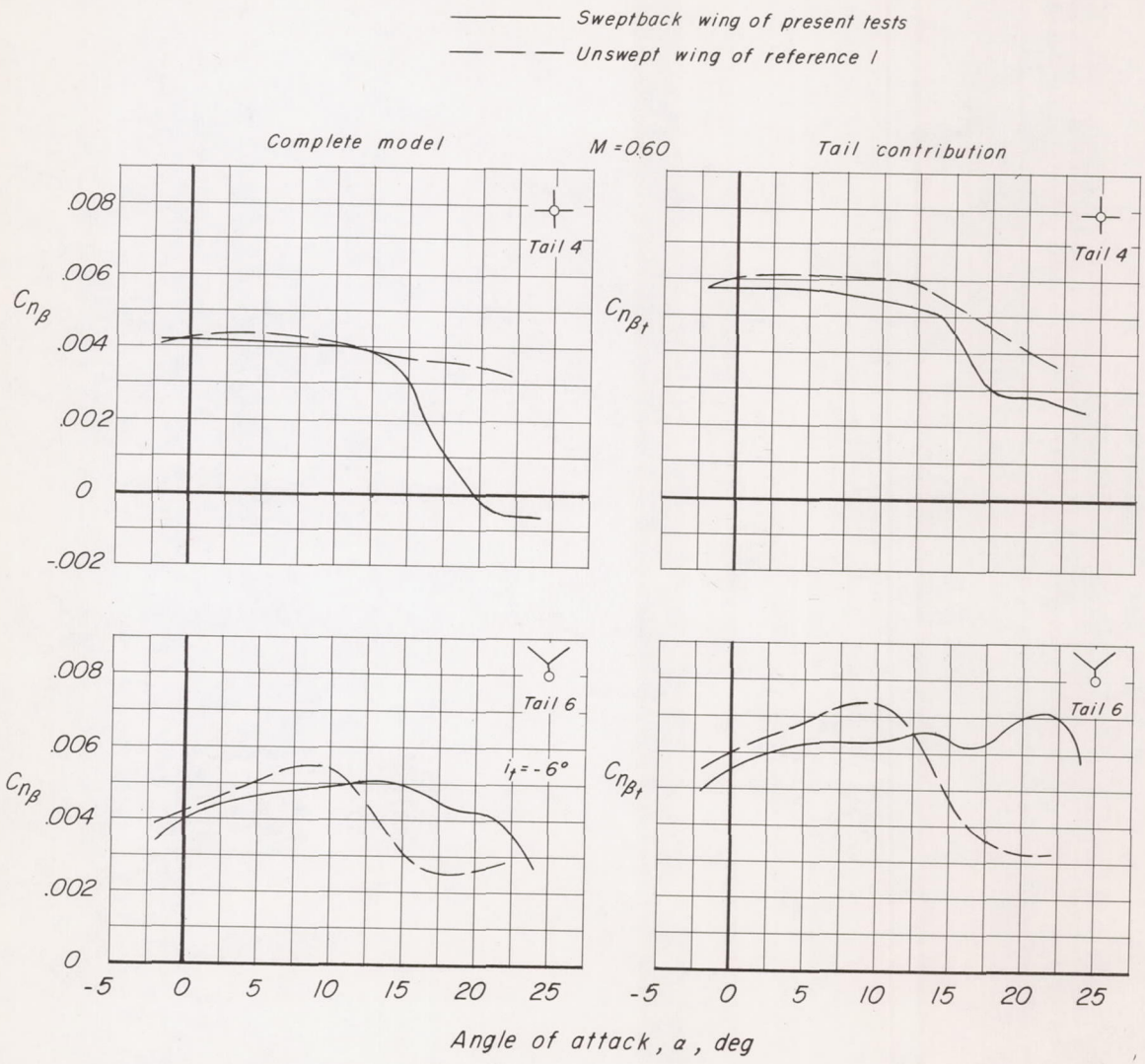

Figure 22.- Comparison of directional stability characteristics of the model having the sweptback wing with the results obtained for the unswept wing of reference 1. $i_t = 0^\circ$ except as indicated otherwise. (Coefficients are based on geometry of the swept wing.)